Chemical Geology xxx (xxxx) xxx–xxx

Contents lists available at ScienceDirect

Chemical Geology

journal homepage: www.elsevier.com/locate/chemgeo

Invited research article

Vein-type graphite deposits in Sri Lanka: The ultimate fate of granulite fluids

Jacques L.R. Touret[a,*], Jan Marten Huizenga[b,c], K.V. Wilbert Kehelpannala[d], Francesca Piccoli[a]

[a] Institut de Minéralogie, Physique des Matériaux, Cosmochimie, Sorbonne Universités, 4 Place Jussieu, F-75005 Paris, France
[b] Economic Geology Research Institute (EGRU), College of Science and Engineering, James Cook University, Townsville, Queensland 4811, Australia
[c] Department of Geology, University of Johannesburg, Auckland Park, 2006 Johannesburg, South Africa
[d] Department of Geology, Faculty of Science, University of Botswana, Private Bag UB00704, Gaborone, Botswana

ARTICLE INFO

Keywords:
Sri Lanka
Hydrothermal vein graphite
Granulite
CO_2 fluid
High salinity brine
Lower crust

ABSTRACT

Hydrothermal graphite vein deposits hosted in granulite facies metamorphic rocks in Sri Lanka are unique because of their large size and high crystallinity. In this paper, we present a review of the structural-metamorphic setting of the graphite veins and of the graphite stable carbon isotope data, and we present fluid inclusion data from quartz in the graphite veins and in the host rocks from several graphite deposits in Sri Lanka. The studied host rocks show decompression rims of plagioclase and orthopyroxene after garnet. The quartz in these decompression rim textures comprise, in order of abundance, high-salinity brine, H_2O-CO_2, and low-salinity aqueous fluid inclusions. The brine fluid is responsible for metasomatic features observed in garnet decompression rims, including feldspar leaching and re-precipitation. Quartz cogenetic with vein graphite comprises, in order of abundance, low-salinity aqueous, CO_2, high-salinity brine, and H_2O-CO_2 fluid inclusions. Published graphite carbon isotope data indicates a dominant mantle source, mixed with small amounts of carbon-bearing fluids of supracrustal origin. We propose that large quantities of mantle-derived CO_2 fluid are temporarily stored in the lower crust during the final stage of Gondwana supercontinent amalgamation. The CO_2 is subsequently released from the lower crustal rocks during decompression associated with fast uplift. The graphite veins in Sri Lanka were formed during this uplift stage and represent as such paleofluid channels. In this respect, they are comparable to the quartz-carbonates mega-shear zones found in other granulite terranes. Depending on the redox conditions, mantle CO_2 and brines may either result in the formation of graphite or quartz-carbonate veins.

1. Introduction

Since the 19th century, Sri Lanka has been one of the major graphite producers in the world, especially for high quality, highly crystalline graphite, containing ca. 95–98 wt% of pure carbon. Other graphite deposits occur in the USA and other parts of former Gondwana, e.g. Madagascar (Kehelpannala, 1993; Luque et al., 2014) and southern India (Soman et al., 1986; Radhika and Santosh, 1996; Sanyal et al., 2009; Luque et al., 2014). The graphite deposits in Sri Lanka, however, are the largest of their kind, occurring in a wide north-south extending belt in the western part of the Precambrian high-grade metamorphic terrains of the island (Dissanayake, 1981; Kehelpannala, 1995, 1999a). Graphite mining in Sri Lanka had its peak during the first half of the 20th century, with over 2500 graphite pits and mines active before World War II (Wijayananda, 1985). Competition with mass production of flake graphite, notably from countries like China and Mexico, resulted in a decrease in mining activities, despite a growing global interest for high-crystallinity graphite. At present, Sri Lanka is the only producer of the high-quality lump and chippy dust graphite varieties, coming from a limited number of underground mines (in particular the Kahatagaha and Bogala mines, see Fig. 1). Graphite-quartz and host rock samples collected from four of those mines were selected for the present study (Fig. 1). The main aims of this study are to (1) present a detailed review of the structural-metamorphic setting and carbon stable isotope geochemistry of Sri Lankan vein graphite, (2) present, for the first time, fluid inclusion data, and (3) discuss the formation of graphite veins and its relationship with the tectono-metamorphic history of the host rocks.

2. Precambrian geology of Sri Lanka

2.1. Lithotectonic units of Sri Lanka

The position of Sri Lanka within East Gondwana, linking India, Madagascar, Africa and east Antarctica, makes this region of prime importance for understanding the mode of formation of the Late

* Corresponding author.
E-mail address: jan.huizenga@jcu.edu.au (J.L.R. Touret).

https://doi.org/10.1016/j.chemgeo.2018.03.001
Received 30 November 2017; Received in revised form 27 February 2018; Accepted 1 March 2018

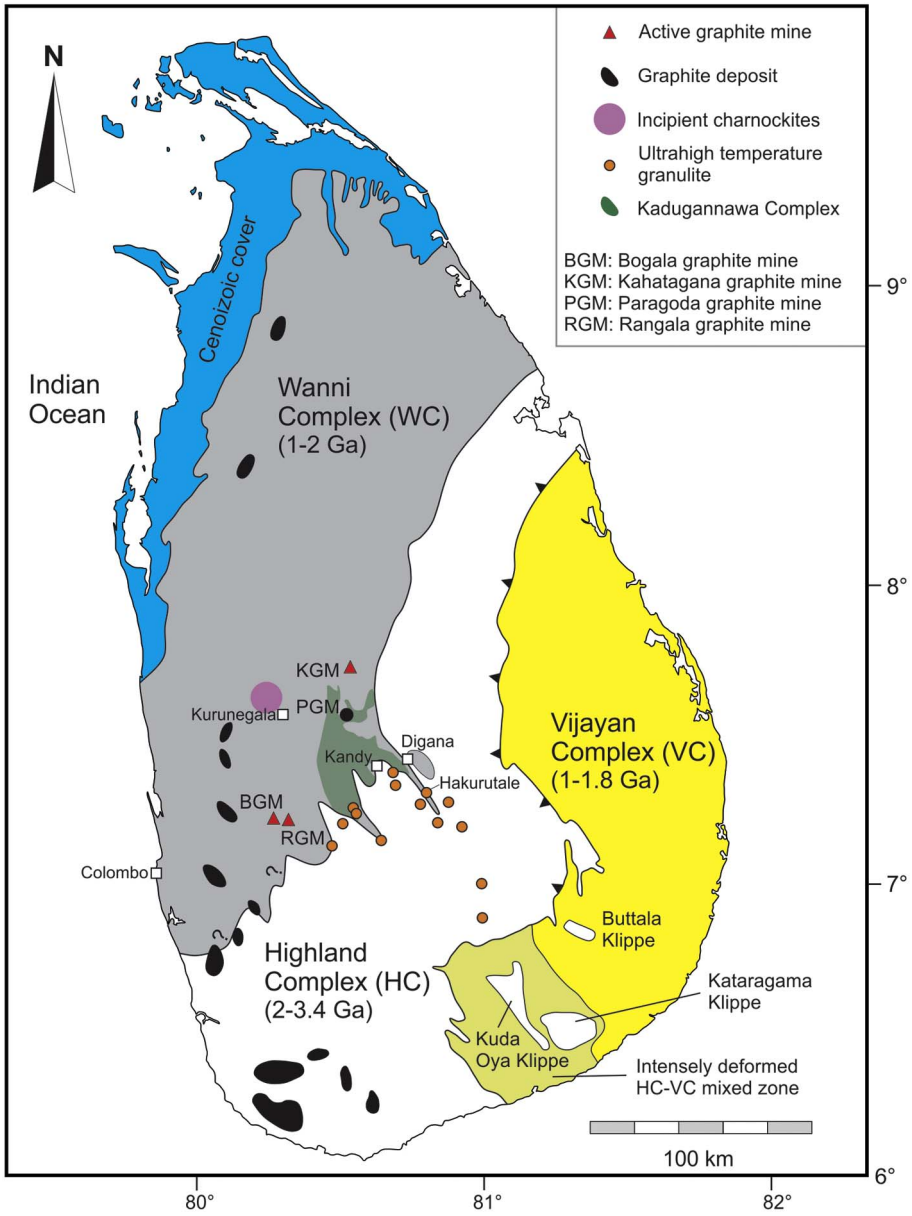

Fig. 1. Geological map of Sri Lanka (modified after Kehelpannala, 1995) showing the three main lithotectonic units and their Nd model ages, and the localities of active graphite mines and major graphite deposits. The Highland-WC boundary is after Kehelpannala (2017a). The northern portion of this boundary is interpreted to be a suture zone (Kröner et al., 2013, and references therein). The map shows the localities for UHT granulites (Dharmapriya et al., 2015; Osenai et al., 2016b; Dharmapriya, 2017), and arrested charnockites (Hansen et al., 1987).

Neoproterozoic Gondwana supercontinent (Yoshida et al., 1992, Yoshida and Santosh, 1994; Santosh et al., 2014; Kehelpannala, 2017a). The various configurations of east Gondwana, positioning Sri Lanka in the central part, have recently been reviewed by Kehelpannala (2017a, 2017b). Except for a thin Cenozoic sedimentary cover along the north-western coastal belt of Sri Lanka (Fig. 1), the whole island comprises Precambrian high-grade metamorphic rocks metamorphosed to upper amphibolite, granulite, and ultrahigh temperature (UHT) granulite facies.

Based on Nd model ages (Milisenda et al., 1988) and U-Pb zircon ages, the Neoproterozoic to Palaeoproterozoic basement of Sri Lanka is subdivided into three lithotectonic units or complexes (Fig. 1, Kehelpannala, 1997), namely the Wanni Complex (WC), the Highland Complex (HC) and the Vijayan Complex (VC). The characteristics of these three complexes are summarized in Table 1. The contacts between the three complexes are generally assumed to be tectonic (Kröner et al., 2013, and references therein). The boundary between the centrally located HC and the VC is a major crustal-scale ductile shear zone representing a suture zone (Kröner et al., 2013, and references therein). The nature and the exact location of the contact between the WC and the HC in the southwest, on the other hand, is uncertain (Kröner et al., 2013).

Kröner et al. (1991) and Cooray (1994) identified the Kadugannawa Complex (Fig. 1) as an addition to the others based on the apparently unique (migmatized) mafic lithologies comprising hornblende and hornblende-biotite gneisses and the presence of doubly plunging synforms. This subdivision has been accepted by numerous researchers including Kröner et al. (2003), Santosh et al. (2014), He et al. (2015, 2016), and Dharmapriya et al. (2017). However, the similarities in Nd model and U-Pb zircon ages, geochemistry (Milisenda et al., 1988, 1994; Kröner et al., 1991, 2003; Willbold et al., 2004; Kehelpannala, 2004), lithologies, and structural geology suggests that the KC is part of the WC (Kehelpannala, 1997). This interpretation has been adopted by Osanai et al. (2006), Kröner et al. (2013), Hiroi et al. (2014), and also in this study.

The vein graphite occurrences of Sri Lanka are located in the

Table 1
Main characteristics of the Wanni, Highland, and Vijayan Complexes in Sri Lanka. Details about the age of metamorphism are given in the text.

Complex	Nd model age	Lithologies	Metamorphism
Wanni	1–2 Ga[1]	Metapelite, quartzite, granitoid gneisses, charnockites, and numerous metamorphosed mafic igneous rocks. Marble is notably absent[1,2].	Granulite-facies metamorphism at 5–7 kbar, 700–830 °C[3]. Metamorphic evolution is characterized by a clockwise *P-T* path[3]. In-situ charnockitisation occurred at 5–6 kbar and 700–750 °C[4].
Highland	2–3.4 Ga[1]	Dolomitic marble, marble, meta-calcsilicate gneiss, metapelite, quartzite, charnockite, enderbite, and numerous metamorphosed mafic igneous rocks[1,2].	Granulite-facies metamorphism up to 900 °C at ca. 8 kbar[5]. Localised UHT metamorphism at 9–12.5 kbar and 900–1150 °C[6,7,8,9,10]. Metamorphic evolution for non-UHT and UHT granulites is characterized by a clockwise *P-T* path[3,9,10].
Vijayan	1–1.8 Ga[1]	Dominated by migmatites, granitoid gneisses with minor amphibolite, quartzite, and meta-calcsilicate[1,2].	Granulite-facies metamorphism (ca. 8 kbar, 800–850 °C)[11] is followed by extensive retrogression at amphibolite facies metamorphic conditions. The shape of the *P-T* path is unknown.

[1] Milisenda et al. (1988, 1994).
[2] Cooray (1994).
[3] Raase and Schenk (1994).
[4] Perchuk et al. (2000).
[5] Dharmapriya et al. (2014).
[6] Sajeev and Osanai (2004).
[7] Osanai et al. (2006).
[8] Osanai et al. (2016a).
[9] Dharmapriya et al. (2015).
[10] Dharmapriya et al. (2017).
[11] Kleinschrodt (1994).

western part of the country (Kehelpannala, 1995, 2017b) in both the WC and HC (Fig. 1). It is noteworthy that graphite formation post-dates the granulite facies metamorphism of both the WC and the HC (Kehelpannala, 1993, 1995, 1999a). Most graphite deposits are within distance of ca. 15–30 km of the WC-HC boundary and approximately aligned parallel to this boundary (Fig. 1). It is also interesting to note that some vein graphite deposits in the Kurunegala area in the WC are located near the "incipient charnockite" occurrences (Fig. 1) (Hansen et al., 1987; Kehelpannala, 1999b; Perchuk et al., 2000).

2.2. High-grade metamorphism in Sri Lanka

2.2.1. Age of metamorphism

The age constraints of the metamorphic events of the different complexes have been the subject of many studies. The main granulite-facies metamorphic event in the HC, based on Rb-Sr whole-rock isochron ages was initially considered to be Late Mesoproterozoic (1100 Ma, Cordani and Cooray, 1989) or Palaeoproterozoic (1930 Ma, De Maesschalck et al., 1990). Single zircon dating (summarized in Santosh et al., 2014 and in Dharmapriya et al., 2016) documents Archaean to Palaeoproterozoic ages (3.2–2.4 Ga) for detrital zircons from the HC metasediments (Kröner et al., 1987). Studies by Santosh et al. (2014) and He et al. (2015) indicate repeated thermal events during most of the Neoproterozoic (between 1000 and 600 Ma). Available zircon U-Pb ages suggest that all magmatic rocks and metasediments in both the WC and HC have been metamorphosed under amphibolite to granulite facies conditions at ca. 620–535 Ma (Kröner et al., 1994; Kröner and Jaeckel, 1994; Kröner and Williams, 1993; Santosh et al., 2014; Dharmapriya et al., 2016; Osanai et al., 2016a). Zircon metamorphic ages derived from various lithologies in both the WC and HC record at least two thermal events at ca. 620–580 Ma and 560–535 Ma (Santosh et al., 2014; Dharmapriya et al., 2016; Osanai et al., 2016a).

The age of the UHT metamorphic event has been a matter of debate. Sajeev et al. (2003) obtained a Sm-Nd whole-rock isochron age of 1478 ± 58 Ma, inferring that UHT granulites could be relics of a pre-Pan African metamorphism. However, a U-Pb zircon metamorphic age of ca. 580 Ma from relatively high-pressure mafic UHT granulites (Sajeev et al., 2007) as well as zircon and monazite ages of ca. 570 Ma from sapphirine granulites (Sajeev et al., 2010) have led these authors to revise their earlier views and to consider, like most authors working in the region, that UHT metamorphism is Pan-African (Eocambrian) in age and coeval with the amalgamation of the Gondwana supercontinent.

Baur et al. (1991) dated arrested charnockite-host orthogneiss pairs exposed in the Udadigana quarry, Kurunegala and obtained an upper intercept age of 771 Ma, which they interpreted to be the intrusive age of the original rock. Burton and O'Nions (1990) obtained U-Pb ilmenite-whole rock isochron ages of 1094 ± 8 and 1095 ± 4 Ma, respectively, on two samples of the original orthogneiss from the Waraddana quarry occurring north of Udadigana. On the basis of small-domain Sm-Nd and Rb-Sr whole-rock data from arrested charnockite from the same quarry, Burton and O'Nions (1990) suggested that in-situ charnockitization occurred at ca. 535 Ma, i.e. the charnockitization event post-dates the main metamorphic event (Kehelpannala, 1999b) by not more than ca. 30 Ma.

2.2.2. Metamorphic P-T conditions and UHT metamorphism

The VC records upper amphibolite- to granulite-facies metamorphism with estimated peak *P-T* conditions of ca. 8 kbar and 800–850 °C, respectively (Kleinschrodt, 1994; Kröner et al., 2013). Peak *P-T* conditions in the WC are slightly lower: 5–7 kbar and 700–830 °C (Schenk et al., 1991; Raase and Schenk, 1994), respectively. The HC shows an increase in metamorphic *P-T* conditions from 4.5–6 kbar and 700–750 °C in the southwest to 8–9 kbar and 800–900 °C in the southeast (Dharmapriya et al., 2014; Dharmapriya et al., 2017, and references therein). Both the WC and HC are characterized by clockwise *P-T* paths (Raase and Schenk, 1994; Dharmapriya et al., 2017, and references therein).

A significant feature of the HC is the occurrence of UHT granulites (Sajeev and Osanai, 2004; Osanai et al., 2006) in the central part (Fig. 1) along the folded suture zone between the WC and the HC (Dharmapriya, 2017). The UHT granulites comprise typical UHT mineral assemblages (particularly in Mg-rich lithologies), including sapphirine-kyanite, orthopyroxene-sillimanite-quartz, and osumilite-spinel-quartz (e.g., Sajeev and Osanai, 2004; Dharmapriya et al., 2015; Osanai et al., 2016a). Peak *P-T* conditions were estimated to be 9–12.5 kbar and 900–1150 °C, respectively (Sajeev and Osanai, 2004; Sajeev et al., 2007; Osanai et al., 2006, 2016a). Like for the WC and the non-UHT granulites in the HC, a clockwise *P-T* path characterizes UHT granulites in the HC (Dharmapriya et al., 2015).

Rocks with suitable composition in both the WC and HC show evidence for decompression as exemplified by the breakdown of garnet according to the following reactions (e.g. Schenk et al., 1991; Kehelpannala, 1999a):

$$\text{garnet} + \text{quartz} \rightarrow \text{orthopyroxene} + \text{plagioclase} + \text{Fe} - \text{Ti oxides} \quad (1)$$

garnet + clinopyroxene → orthopyroxene + plagioclase + Fe − Ti oxides (2)

These reactions result in symplectitic orthopyroxene and plagioclase forming a typical decompression rim texture around garnet. Decompression (6.5 to 5 kbar) took place after the main folding event in Sri Lanka at ca. 700–650 °C, i.e. ca. 50–100 °C below the peak metamorphic temperature (Schenk et al., 1991; Dharmapriya et al., 2014). Noteworthy is the presence of spherulitic and dendritic felsite inclusions in garnet in both HC and WC granulites, most of them situated near the HC-WC boundary (Hiroi et al., 2014). Their presence indicates fast uplift in a continent collision environment (Hiroi et al., 2014).

The VC shows a distinct different retrograde evolution compared to the WC and HC, characterized by retrogression associated with pervasive, fluid-induced potassium alteration, which also resulted in the formation of widespread migmatites in the complex (Kröner et al., 2013).

2.2.3. Fluids present during high-grade metamorphism

A major (but rarely mentioned) feature of UHT granulites is the occurrence, in most rock-forming minerals, of a great number of primary high to ultrahigh density CO_2 fluid inclusions, (up to ca. 1.16 g/cm^3) (e.g., Santosh et al., 2004; Santosh and Omori, 2008a; Touret et al., 2016). CO_2 fluid inclusions in sapphirine-bearing UHT granulites (Kriegsman and Schumacher, 1999) in Sri Lanka have been reported by Bolder-Schrijver et al. (2000) and Santosh and Omori (2008a). For example, the sapphirine-bearing granulites of Hakurutale (Fig. 1) located along the folded WC-HC boundary (Fig. 1) demonstrate the presence of significant amounts of CO_2 trapped in fluid inclusions (Bolder-Schrijver et al., 2000) (Fig. 2). Rock-forming minerals such as garnet and pyroxene may contain up to a few weight percent CO_2 trapped in fluid inclusions (e.g., Touret and Hansteen, 1988). The CO_2 fluid is associated with magnesite that occurs as a daughter phase in the fluid inclusions indicating that $MgCO_3$ was a component in the CO_2 fluid (see discussion in Bolder-Schrijver et al., 2000). The association of CO_2 with UHT granulites suggests that mantle CO_2 was transported by magma during peak metamorphism (Touret and Huizenga, 2011) allowing the lower crust to reach near-magmatic temperatures (> 1000 °C) (Kelsey and Hand, 2015). As has been shown for other granulite occurrences, a high-salinity brine fluid is commonly present as well (e.g., Touret and Huizenga, 2011) which is, because of its high salinity (at least 40–50 wt % NaCl equivalent), immiscible with CO_2 even under UHT granulite facies metamorphic conditions. In contrast to CO_2-bearing fluid inclusions, brine fluid inclusions are generally not preserved during retrograde metamorphism. The greater mobility of brine fluids along mineral intergrain boundaries (e.g., Gibert et al., 1998) makes these fluids less susceptible for trapping and preservation in inclusions as has been discussed in detail by Touret (2001) and Touret and Huizenga (2011). Even if brine fluids do get trapped, the steep isochores of brine fluid inclusions most likely result in their (partial) destruction during the isobaric cooling stage of UHT metamorphic rocks (Touret, 2001; Touret and Huizenga, 2011), which in many cases precedes uplift and decompression. The existence of brine fluids is clearly evidenced by typical metasomatism-related microstructures (feldspar microveins, myrmekites) along intergrain boundaries in charnockites and granulites (Harlov et al., 1998; Perchuk et al., 2000; Touret and Huizenga, 2011, 2012; Safonov and Aranovitch, 2014). However, the modification or absence of brine fluid inclusions makes it impossible to determine the exact composition of brine fluids.

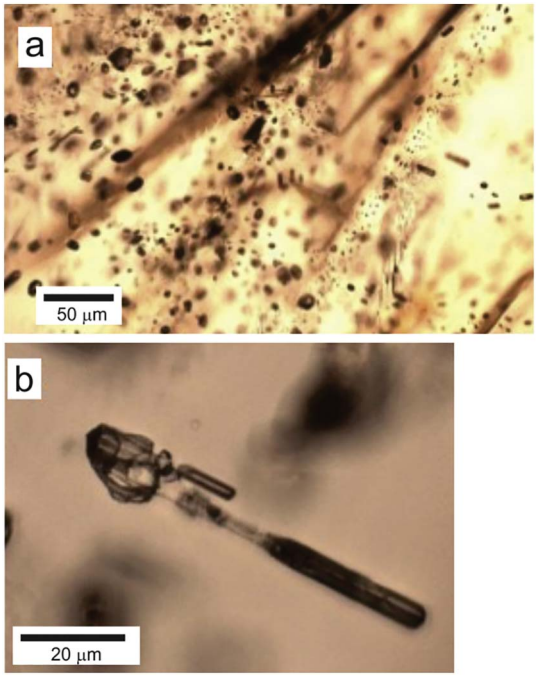

Fig. 2. (a) CO_2 inclusions (dark spots) in sapphirine-bearing ultrahigh-temperature granulite from Hakurutale (Bolder-Schrijver et al., 2000, see Fig. 1 for locality). (b) Detail of an elongated, tubular fluid inclusion. Black part: supercritical, high-density CO_2 (*Th* into the liquid phase at ca. -20 °C); white part: magnesite daughter crystals.

As mentioned earlier, a typical feature of the WC is the presence of incipient charnockites (e.g., Hansen et al., 1987). They are the result of local transformation of amphibolite-facies gneisses into a homogeneous charnockite. The classical Kurunegala occurrence (Fig. 1) has been studied in detail by Hansen et al. (1987) and Perchuk et al. (2000). Elongated patches of dark greenish charnockites formed along a system of small-scale ductile shear zones and rarely along foliation planes in grey-white quartzofeldspathic gneisses (e.g., Kehelpannala, 1999b). They vary in length between 10 cm up to a few meters and have a thickness of 10–20 cm. The charnockite patches show a decrease in biotite and hornblende and an increase in orthopyroxene content, while the grain size of K-feldspar increases. Evidence for alkali metasomatism, especially feldspar microveins along quartz-feldspar intergrain boundaries or myrmekites, is widespread. Remnants of brine inclusions have been found in and near these microveins, together with rare CO_2 inclusions (Perchuk et al., 2000; Touret and Huizenga, 2012). Charnockitization occurs in presence of fluid with a H_2O activity of 0.6 (Perchuk et al., 2000) at *P-T* conditions of 650–750 °C and 5–6 kbar, respectively. An H_2O activity of 0.6 relates to high-salinity brine fluid (ca. 50 wt% NaCl equivalent, Aranovich and Newton, 1996) or a H_2O-CO_2 fluid (ca. 50 mol% CO_2, Aranovich and Newton, 1999).

2.3. Tectono-metamorphic evolution of Sri Lanka

Kehelpannala (2004) and Santosh et al. (2014) have presented models explaining the tectono-metamorphic evolution of Sri Lanka. Kehelpannala (2004) (Fig. 3a) proposed that the WC, HC, and VC were three distinctly different crustal domains that amalgamated during the Late Neoproterozoic Gondwana assembly by two separate collision events following two separate subductions. According to this model, the WC seems to have formed as part of root zone of an Andean-type magmatic arc whereas the VC may have originated as part of an island arc (Kehelpannala, 2004). The subduction of the HC microcontinent under the WC magmatic arc led to the first collision between the WC and the HC. The subsequent subduction of the oceanic plate carrying the VC island arc under the united WC-HC block brought these three units into contact during the second collision (Kehelpannala, 2004). In this model, granulite facies metamorphism in both the WC and HC are related to the first collision and the high-grade metamorphism reported in the VC is related to the second collisional event.

Santosh et al. (2014) speculated, in order to link the HC to the metasedimentary terrains in southern India, that the Late Neoproterozoic-Cambrian HC formed as part of an accretionary complex developed during a Neoproterozoic double-sided subduction involving the

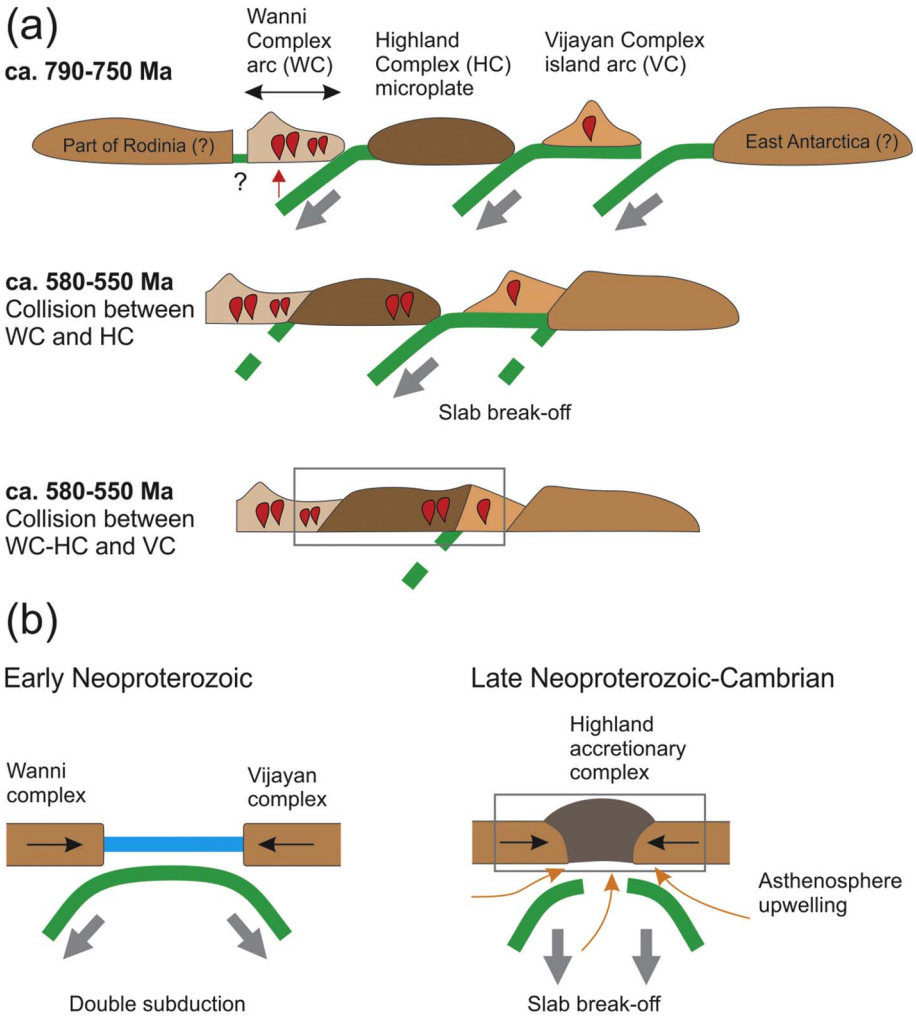

Fig. 3. Tectono-metamorphic models for Sri Lanka. (a) Two-collision model by Kehelpannala (2004). (b) Double subduction model by Santosh et al. (2014). See text for further discussion. The grey rectangle shows the present-day configuration of Sri Lanka.

WC and VC (Fig. 3b). In this model, HC sediments are considered to have deposited as an accretionary complex on a Neoproterozoic ocean between the WC and the VC, and the final collision between these two units during Late Neoproterozoic-Cambrian led to the closure of the ocean creating the HC as a suture zone.

The two-collision model (Kehelpannala, 2004) appears to be the best fit with the available data, including the Late Neoproterozoic-Cambrian metamorphic ages, the large volume of Paleoproterozoic metagranitoids in the HC, the HC klippen occurring in the south-eastern part of the VC (Fig. 1), and the clockwise *P-T* paths of the HC and WC (Raase and Schenk, 1994; Dharmapriya et al., 2017, and references therein). Most of these features are difficult to explain in the double subduction model proposed by Santosh et al. (2014).

3. Nature of graphite veins

Almost all graphite-bearing veins are oriented in an east-west direction and steeply dipping to the south. The thickness of most graphite veins varies from a few mm to a few dm, the thickest being < 1 m. Their horizontal length ranges from a few metres to tens of metres, the longest being over 75 m (Kehelpannala, 1999a). The graphite veins occur in swarms forming extensional en-echelon arrays. The “upward forking” of the graphite veins indicates that they are branching off from a common source area at an unknown depth (Kehelpannala, 1999a).

The graphite veins crosscut gneissic foliations of inhomogeneous granulite-facies rocks of both sedimentary and igneous origin. Most of the host rocks are free of disseminated graphite. The graphite veins also crosscut the axial planes of large-scale synforms and antiforms (Kehelpannala, 1999a) postdating the major folding event, which occurred after peak metamorphism but still at granulite-facies metamorphic conditions (Kehelpannala, 1999a).

In outcrop, the graphite vein boundaries generally appear knife sharp. However, at close inspection it can be observed that the vein forms a series of regularly spaced bulges convex towards the host rock (Fig. 4a, b), which is clearly visible in thin section (Fig. 4c, d). The occurrence of a few garnet remnants in the graphite vein in sample 1KGM1 (top of Fig. 4d) indicates that the graphite split the wall rock.

The graphite veins comprise a wide variety of gangue minerals including quartz, Na-K-feldspar, clinopyroxene, biotite, muscovite, apatite, pyrite, pyrrhotite, chalcopyrite, sphalerite, marcasite, calcite, siderite, dolomite, iron ores and traces of Mn-carbonate (Kehelpannala, 1995, 1999a). Graphite crystals are up to a few cm in size and show fibrous, coarse-flaky, and rosettes crystal shapes. Typically, graphite occurs as fibrous aggregates at the vein edge, becoming elongated crystals intergrown with quartz approximately perpendicular to the vein wall. Massive graphite characterizes the centre of the vein (Kehelpannala, 1993; Katz, 1987). Pyrite is often associated with graphite, either as thin films within the graphite or as fracture coatings within the quartz associated with vein graphite (Katz, 1987). Detailed textural descriptions of the vein graphite by Katz (1987) provide evidence for repetitive events of fracturing and sealing (crack-seal events).

The metamorphic minerals of the host rocks include quartz,

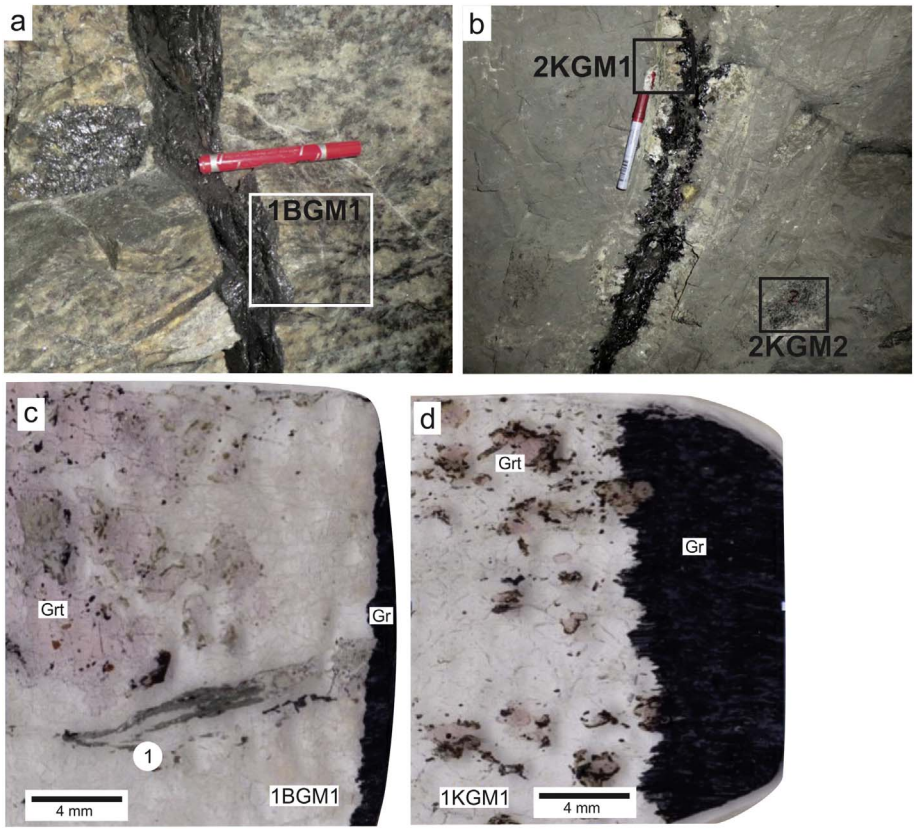

Fig. 4. Illustration of host rock-graphite vein contact. (a) Graphite vein in Bogala mine (sample 1BGM1). (b) Graphite vein in Kahatagaha mine (samples 2KGM1, 2KGM2). (c) Khondalite host rock sample 1BGM1 showing pink garnet and graphite. 1: microshear zone, resembling pseudotachylite cut by the graphite vein indicating that sudden brittle failure was preceded by shearing episodes in dry (H_2O-absent) granulites. (d) Orthopyroxene-bearing garnetiferous quartzofeldspathic gneiss host rock sample 1KGM1 from Kahatagaha. Fibrous graphite is exemplified by the well-developed bulges at the graphite vein boundary. (For interpretation of the references to colour in this figure legend, the reader is referred to the web version of this article.)

plagioclase, K-Na-feldspar, garnet, orthopyroxene, clinopyroxene, hornblende, biotite, calcite and dolomite. Sillimanite occurs in rare pelitic host rock, especially at the Bogala mines. Close to the graphite veins intense wall rock alteration is exemplified by completely or partially obliteration of the rock fabric and alteration of both orthopyroxene and plagioclase, which are produced during decompression (Reactions (1) and (2)). This implies that vein graphite formation took place (or was still taking place) at *P-T* conditions that are lower than those of the decompression reactions (Kehelpannala, 1995). The alteration minerals include antiperthite, chlorite, sphene, Cl-F-apatite, orthoclase, myrmekite, Cl-rich dark brown biotite, Cl-rich hornblende, Cl-scapolite and unidentified Ti-bearing mineral phases (Kehelpannala, 1995). The exsolution of plagioclase, forming antiperthite in the wall rock alteration zones is unique to the Sri Lankan vein graphite and is found in all altered rocks (including altered basic rocks) (Kehelpannala, 1999a). The alteration of a thin calcsilicate rock layer from the Bogala mine excludes the involvement of carbonate carbon in the origin of vein graphite (Kehelpannala, 1999a).

The occurrence of graphite deposits within granulite facies rocks in Sri Lanka has led Katz (1987) to propose that graphite precipitated from a CO_2 fluid at granulite facies metamorphic conditions. However, as discussed earlier, the graphite veins post-date peak metamorphism excluding this as a possibility (Kehelpannala, 1995, 1999a; Kehelpannala and Francis, 2001).

3.1. Carbon source for graphite: Stable isotopes

The origin of graphite in granulites is a long-standing problem (Luque et al., 2014). Graphite occurs frequently as an accessory or even rock-forming mineral in high-grade metamorphic rocks (e.g., Luque et al., 2014). It typically occurs as disseminated flakes in metapelites or in association with carbonate minerals in marbles (Landis, 1971; Nokleberg, 1973). In the first case, carbon is derived from organic matter in the sediment protoliths (Landis, 1971) and redistributed by hydrothermal fluids during metamorphism (Rumble III et al., 1986, Rumble, 2014). Graphite in marbles is also of supracrustal origin and derived from the reduction of carbonates or carbonaceous matter (Weis et al., 1981). In this case, carbon is immobile suggesting a fluid-absent environment, which is indicated by the persistence of carbonate metasedimentary rocks at granulite facies *P-T* conditions. The graphite flakes in metapelites show a relatively light carbon isotope signature, indicative of biogenic origin despite the complexities of fluid-mineral interaction with relatively low $\delta^{13}C_{PDB}$ values of ca. −25‰ (Luque et al., 2012, 2014). The $\delta^{13}C_{PDB}$ values from graphite in marbles are heavier and close to ca. 0‰ (Luque et al., 2012, 2014).

The isotope composition of vein graphite in Sri Lanka has been the subject of numerous studies (Dobner et al., 1978; Weis et al., 1981; Binu-Lal et al., 2003; Touzain et al., 2010; Luque et al., 2012, 2014). Reported $\delta^{13}C_{PDB}$ values of graphite range from −6 to −10‰, with slight variations across the vein. Graphite in contact with the host rocks shows a $\delta^{13}C_{PDB}$ value of −9.4‰ whereas graphite in the centre shows a $\delta^{13}C_{PDB}$ value of −10.3‰ (Hoernes et al., 1994; Touzain et al., 2010; Luque et al., 2014). The progressive change of a relatively light core (−13‰) to a heavier rim (−8.5‰) has also been observed by Santosh and Wada (1993) within a single graphite crystal in a khondalite from southern India. Vein graphite $\delta^{13}C_{PDB}$ values are significantly higher than those for disseminated graphite in the khondalite host rocks ($\delta^{13}C_{PDB}$ values between −12 and −18‰). Variable $\delta^{13}C_{PDB}$ values of −8.1‰, −15.9‰ and −16.3‰ are obtained from disseminated graphite from three different metapelite samples from the southwestern part of the HC near vein graphite deposits (Fig. 1). The isotopic variation can be interpreted as a result of biogenic graphite in the khondalite proto-sediment that is overgrown by graphite derived from a heavier mantle CO_2 fluid (Luque et al., 2014).

Carbon isotopes from different generations of graphite in rocks from the Digana shear zone provides valuable additional information (Binu-Lal et al., 2003). Shear zones are widespread in and around most granulite terranes and range from small-scale ultramylonites and

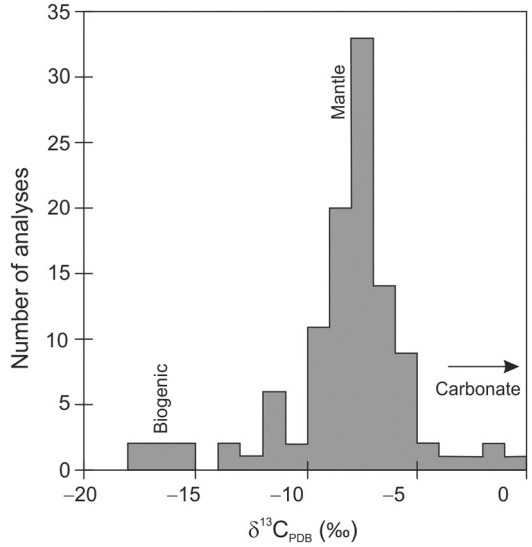

Fig. 5. Histogram (modified from Binu-Lal et al., 2003) showing a compilation of carbon stable isotope compositions of graphite from Digana, Bogala mines and adjacent areas (near Kandy). Data are from Dobner et al. (1978), Elsenheimer (1988), Fiorentini et al. (1990), Hoernes et al. (1994), Binu-Lal et al. (2003), and Touzain et al. (2010).

pseudotachylites (Clarke and Norman, 1993) to crustal-scale shear zones of subcontinental size (cf. Madagascar, Pili et al., 1999). As such, they are ideal conduits for lower crustal and mantle fluids. Graphite in the Digana metagranitoid mylonites shows $\delta^{13}C_{PDB}$ values varying between −6.3 and −7.9‰, with the exception of small amount of graphite in the migmatitic quartzofeldspathic vein (Binu-Lal et al., 2003). These values indicate mantle-derived CO_2 as a possible source.

A compilation of > 100 graphite $\delta^{13}C_{PDB}$ analyses from Digana and other regions of Sri Lanka, including the HC, the WC, and the Bogala and Kahatagaha graphite mines (Fig. 5, modified after Binu-Lal et al., 2003) shows a clear maximum at a $\delta^{13}C_{PDB}$ mantle value of ca. -8‰. This maximum is flanked by two domains with fewer measurements towards very light $\delta^{13}C_{PDB}$ (ca. −18‰) indicating biogenic carbon and heavy $\delta^{13}C_{PDB}$ values (ca. 0‰) probably from carbonate carbon.

In conclusion, the carbon stable isotope studies show that the carbon of Sri Lankan graphite is derived from the mantle with a minor contribution from crustal carbon. Numerous studies have shown that CO_2 trapped in fluid inclusions are mantle derived (e.g. Hoefs and Touret, 1975; Jackson et al., 1988; Dunai and Touret, 1993). We can, therefore, conclude that Sri Lankan vein graphite was either related to a direct influx of mantle CO_2 (Kehelpannala, 1999a) or alternatively related to a release of mantle CO_2 that was temporarily stored in lower crustal granulites. The crustal carbon can be derived either from the oxidation of organic matter or from the reduction of carbonate sedimentary rocks.

4. Fluid inclusions in host rocks and in quartz associated with vein graphite

Considering the numerous papers devoted to regional geology, geochemistry, and metamorphic petrology of the Precambrian rocks in Sri Lanka, the lack of any fluid inclusion data is remarkable, bearing in mind the obvious hydrothermal character of the graphite veins (Katz, 1987; Kehelpannala, 1999a). The paper by Luque et al. (2014) is, to our knowledge, the only one that describes fluid inclusions in quartz associated with vein graphite (Bogola mine), i.e. trailbound H_2O-CO_2 fluid inclusions associated with graphite-bearing cavities.

For the purpose of this study, samples from host rocks and from quartz in graphite veins from four large graphite mines (of which three are still active) in Sri Lanka were studied (Fig. 1, Table 2). These include the Paragoda and Kahatagaha mines north-northwest from Kandy (Fig. 1), and the Bogala and Rangala mines southwest of Kandy (Fig. 1). The graphite veins in these mines are either massive or contain, in addition to quartz, a number of gangue minerals including pyrite, chalcopyrite, carbonates and apatite as mentioned previously in Section 3.

Doubly polished samples (ca. 150 μm thick) were used for microthermometry using a Linkam heating-freezing stage. Pure CO_2 and H_2O inclusions in quartz were used for calibration at the triple points of CO_2 (−56.6 °C) and H_2O (0.0 °C). Critical homogenization temperatures of synthetic H_2O inclusions in quartz were used for calibration at 374 °C. Final CO_2 melting temperatures (*T*m) and CO_2 homogenization temperatures (*T*h) have an accuracy of ± 0.2 °C, homogenization measurements of aqueous inclusions have an accuracy of ± 5 °C.

Phase transitions were measured during heating and include final melting of CO_2 and ice, clathrate dissociation, and homogenization into the liquid phase of CO_2 and aqueous fluid inclusions. The program BULK (Bakker, 2003) was used to calculate the CO_2 molar volume from the homogenization temperature. Isochores for CO_2 were calculated using the equation of state from Zhang and Duan (2009). Salinity, density and isochores for H_2O-NaCl fluid inclusions were calculated using Hokie_Flincs_H_2O-NaCl (Steele-MacInnis et al., 2012). Raman analyses were conducted with a WITec Alpha Access 300 at the Advanced Analytical Centre at James Cook University. The Raman is equipped with a green laser with an excitation wavelength of 532 nm.

4.1. Host rock descriptions

The host rocks of the Bogala and Rangala graphite deposits are garnet-biotite quartzofeldspathic gneiss, metadiorite and minor garnet-sillimanite-graphite gneiss (khondalite), and calcsilicate gneiss (Kehelpannala, 2017b). The host rocks of graphite veins in the Kahatagaha mine are orthopyroxene-bearing garnetiferous quartzofeldspathic gneiss and minor metabasite. The main rock types at the Paragoda deposit include quartzofeldspathic gneiss and metagranite. Some of the garnet-sillimanite gneisses (e.g., sample 2BGM2, Bogala) mapped outside the mines contains a great abundance of prismatic sillimanite, which, together with the equally abundant garnet, gives the rock a pronounced restitic character. The texture is that of a typical granulite, with a strong stretching lineation defined by elongated and flattened quartz crystals, referred to as “plattenquartz” (Fig. 6a).

From each mine, gangue mineral quartz with intergrown graphite and granulite host rocks were sampled at the levels of operation during the year 2013 (at the adit level of the Rangana mine, at the 124 m level of Bogala and at 340 m and 270 m levels of Kahatagaha). In addition, samples of gangue quartz with graphite from the dumping sites of the Paragoda and Bogala mines were collected. Table 2 shows the details of the samples used in this study.

The khondalites in the different mines are similar, with some minor differences, e.g. there is more garnet and evidence of partial melting in khondalite host rock at Bogala, whereas there is more biotite and less garnet in host rock khondalite from Kahatagaha. Some samples (e.g., sample 2KGM1 from Kahatagaha) show a clear migmatite texture of mm-thick fine-grained garnet-rich layers, separated from each other by coarse-grained leucocratic quartz-K-feldspar-plagioclase layers. We will concentrate in this study on samples from the Bogala and Kahatagaha mines.

Bogala sample 2BGM2 (Fig. 6) is a typical garnet-sillimanite-bearing khondalite, containing a large amount of sillimanite aligned in a plattenquartz-defined foliation plane (Fig. 6a). Garnet in this sample shows a core comprising small dark solid inclusions, together with larger clear, rounded quartz inclusions. The small dark inclusions are made of an aggregate of minute mineral grains, less than a few micron in size, in which quartz and feldspar can be identified (Fig. 6b). They can be interpreted as recrystallized melt inclusions in granulites, also referred to as “nanogranites” as described by Cesare et al. (2009) in migmatites and granulites from Kerala.

Table 2
Information of samples used in this study. Mineral abbreviations after Whitney and Evans (2010).

Sample number	Mine	Brief description
1BGM1	Bogala	Contact between Gr vein and Grt-Bt bearing quartzofeldspathic gneiss host rock (sampled at 124 m level). Qz-Fsp layers in the gneiss form a migmatic texture. Abundant Mc is present
2BGM2	Bogala	Khondalite host rock (sampled at 124 m level) sampled ca. 20 cm above the Gr vein.
3BGM1	Bogala	Large Qz crystals comprising Gr from a Gr vein collected from the dump site
3BGM2	Bogala	Large Qz crystals comprising Gr from a Gr vein collected from the dump site
3BGM3	Bogala	Gr-Bt gneiss comprising a part of the Gr vein collected from the dump site
1KGM1	Kahatagaha	Host rock (sampled at 340 m level). Grt-Qz-Fsp gneiss trapped in Gr vein
1KGM2	Kahatagaha	Qz from Gr vein and Grt-Qz-Fsp-bearing host rock sampled at 270 m level
2KGM1	Kahatagaha	Coarse-grained Qz-Mc-Gr from Gr vein sampled at 270 m level
2KGM2	Kahatagaha	Grt-Bt quartzofeldspathic gneiss host rock ca. 20 cm away from Gr vein sampled at 270 m level
3KGM1	Kahatagaha	Large Qz crystal in Gr vein collected from the dump site
1PGM1	Paragoda	Qz from Gr vein
1RGM1	Rangala	Qz from small Gr vein, with interstratified idiomorphic Bt and Gr
1RGM2	Rangala	Fine-grained granulite host rock sampled ca. 20 cm above Gr vein
2RGM1	Rangala	Qz from Gr vein
2RGM2	Rangala	Fine-grained granulite host rock comprising pegmatoid segregations. Gr occurs on coarse Fsp cleavage planes. Sample taken ca. 40 cm above Gr vein

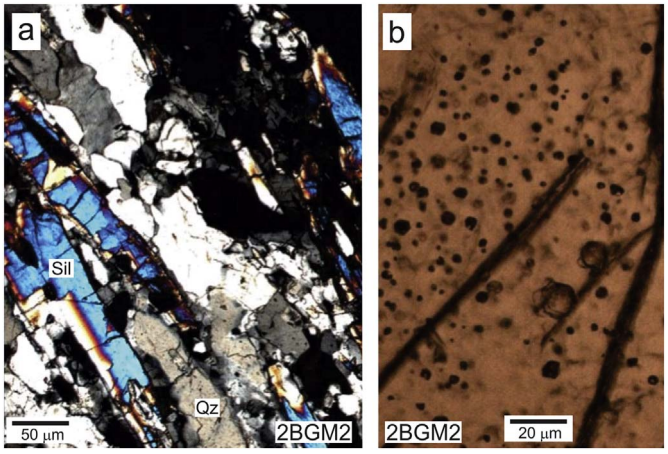

Fig. 6. Sillimanite-bearing khondalite in sample 2BGM2 from Bogala. (a) Typical texture (crossed polarized light) showing prismatic sillimanite appearing as crystals with second-order blue interference colours parallel to foliation and elongated flattened quartz (plattenquartz) with first order grey-white interference colours. (b) Recrystallized melt inclusions in garnet core. (For interpretation of the references to colour in this figure legend, the reader is referred to the web version of this article.)

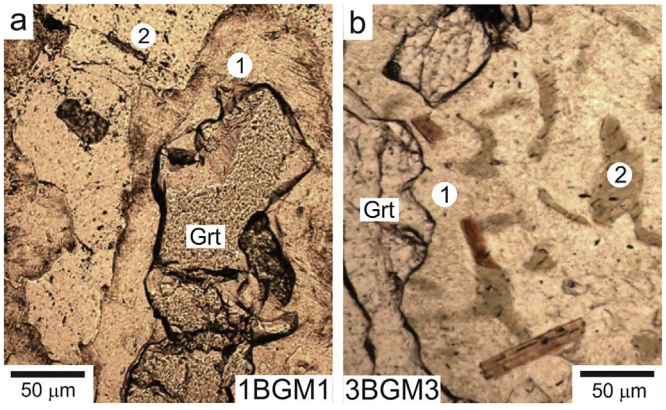

Fig. 7. Photomicrographs (plane polarized light) illustrating garnet decompression textures in samples from Bogala. (a) Photomicrograph (plane polarized light) showing decompression rim around corroded garnet in sample 1BGM1. 1: plagioclase rim; 2: large, undeformed quartz. (b) Photomicrograph (plane polarized light) of sample 3BGM3 showing a large altered plagioclase in the decompression texture (1) and several generations of biotite (2).

Samples 1BGM1 (Bogala, Fig. 4a, c) and 1KGM1 (Kahatagaha, Fig. 4d) were collected at the contact of two different graphite veins. Both samples are garnet-bearing metapelite and associated with the khondalite, except that sillimanite is notably absent. Partial melting is indicated by the relatively large amount of garnet, but no melt inclusions were identified in these rocks.

The most prominent textural feature in all khondalites and garnetiferous quartzofeldspathic gneiss is the occurrence of decompression reaction rims around garnet, comparable to those found elsewhere in Central Sri Lanka as described by Schenk et al. (1991). In the present case, the decompression texture is characterized by an almost continuous rim of plagioclase (altered to orthoclase), together with other minerals including orthopyroxene and Fe-Ti oxides. Their extent is quite variable, from a thin rim around corroded garnet (1 in Fig. 7a) to a broad zone in which only a few garnet crystals are left (Fig. 7b). In samples near the graphite veins (sample 3BGM3), garnet has almost been completely consumed (Fig. 7b) and often plagioclase in the decompression rim is replaced by fine-grained sericite. In the larger decompression rims, altered plagioclase (1 in Fig. 7b) is accompanied by regularly spaced, green-brown pleochroic biotite (2 in Fig. 7b). The decompression rims are surrounded by large, undeformed quartz crystals (2 in Fig. 7a), which appear similar to the quartz segregations found in some graphite veins (e.g., samples 3BGM1 and 3BGM2). Sample 1KGM1 shows a rim of intergrown plagioclase-K-feldspar, in roughly equal volume proportions (i.e., mesoperthite) around garnet. Antiperthite may also occur in some alteration zone associated with graphite veins as described by Kehelpannala (1999a).

There is ample evidence that these mineralogical changes occurred in the presence of fluids. This information is obtained not only from fluid inclusions, as will be discussed later, but also from the presence of intergranular orthoclase microveins. Feldspar microveins are common in granulites and document the migration of brine fluids along intergrain boundaries (e.g., Harlov et al., 1998). Here, feldspar microveins are common around antiperthite crystals in the decompression textures in sample 1KGM1 (Fig. 8a) and resemble those found in incipient charnockites at Kurunegala (Perchuk et al., 2000) (Fig. 8b).

Alkali metasomatism described from the alteration zones around graphite veins (Kehelpannala, 1995) (Fig. 9a) is exemplified by the alteration of plagioclase to, initially antiperthite, and then sericite (sample 3BGM3). Another example involves leaching out of plagioclase (Fig. 9b, sample 1KGM1). Here, the breakdown of garnet (Reaction (1)) results in a decompression texture around garnet (1 in Fig. 9b) that comprises regularly-spaced, subidiomorphic plagioclase crystals separated by orthopyroxene needles growing perpendicular to the garnet grain boundary. The leaching of plagioclase caused orthopyroxene needles being pulled together forming an intricate texture. Dissolved material subsequently precipitates in the outer part of the aureole (3 in

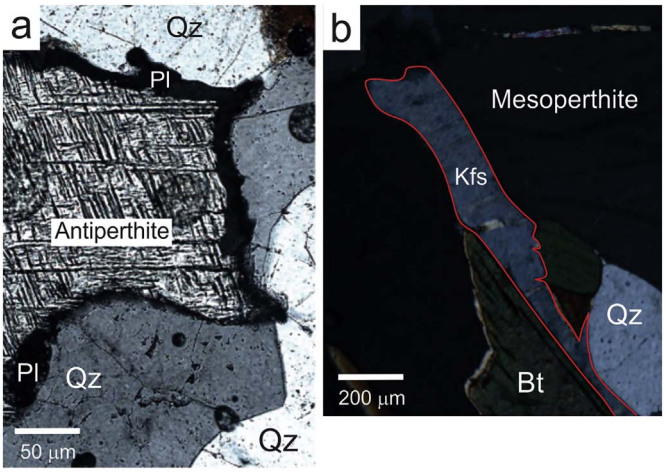

Fig. 8. Photomicrographs (crossed polarized light) showing feldspar microveins developed at grain boundaries. (a) Continuous plagioclase rim at extinction around antiperthite surrounded by quartz (white-grey interference colours) in sample 1KGM1 from Kahatagaha (crossed polarized light). (b) K-feldspar microvein (red outline) developed along grain boundaries in Kurunegala incipient charnockites (Perchuk et al., 2000).

Fig. 9b) in a confuse mass of strongly altered crystals including large, idiomorphic biotite.

4.2. Fluid inclusions in host rocks

Fluid inclusions in host rocks near the graphite veins adds supporting evidence on the nature of fluids involved in graphite vein formation and the associated metasomatic processes. In Bogala (sample 1BGM1), quartz rims within the decompression texture unfortunately comprise only a few fluid inclusions. Fluid inclusions are more abundant in undeformed quartz crystals outside the decompression rim. Overall, four fluid inclusion types were identified in host rocks samples from Bogala and Kahatagaha (Fig. 10).

The first fluid inclusion type represents a low-salinity aqueous fluid (Fig. 10a). The fluid inclusions (5–10 µm) appear as negative crystal shaped liquid-vapour fluid inclusions, either isolated or aligned along intragranular trails (trail terminology after Van den Kerkhof and Hein, 2001, and references therein). They contain a tiny vapour bubble freely moving in a liquid. Initial melting at ca. -20 °C and final melting of ice between −1 and 0 °C indicates a low salinity (< 2 wt% NaCl). Liquid homogenization occurs between 150 and 200 °C. In some cases, a tiny black solid phase is attached to the vapour bubble, which is most probably graphite.

The second fluid inclusion type is characterized by clusters of relatively large (ca. 20–30 µm) regular and irregular shaped H_2O-CO_2 fluid inclusions (Fig. 10b). Melting of CO_2 occurs at −56.6 °C, CO_2 liquid homogenization occurs at ca. +30 °C (i.e., density of the CO_2 phase is 0.59 g/cm^3). The variable water volume fraction from almost zero up to 50 vol% indicates post-trapping modification. Consequently, it is difficult to estimate the fluid composition, the best proxy would be to use the H_2O-CO_2 fluid inclusions with a maximum H_2O content (50 vol% H_2O) corresponds to CO_2 concentration of ca. 20 mol%.

The third fluid inclusion type represents a high-salinity brine fluid. The fluid inclusions occur as decrepitated isolated, intragrain, and transgranular trail-bound fluid inclusions. Small vapour bubbles are present in some satellite fluid inclusions and frequently accompanied by distinct very small halite cubes (1 and 2 in Fig. 10c). Larger halite cubes occur on the walls of larger, dark empty inclusions (3 in Fig. 10c) and are only visible when facing the empty cavity, the refractive index of halite is similar to that of the host quartz. These fluid inclusions represent a high-salinity brine and are most likely related to the metasomatic changes observed in the decompression textures (Fig. 9a, b).

The fourth and final fluid inclusion type is characterized by clusters of a few dark, relatively large (20–30 µm) monophase inclusions (1 in Fig. 10d) surrounded by a swarm of very small (less than one micron in size) colourless fluid inclusions (2 in Fig. 10d). Some of the larger monophase fluid inclusions show irregular shapes indicating decrepitation (1 in Fig. 10d). No phase transitions during heating-freezing experiments were observed in the monophase inclusions so either they comprise very low density CO_2 or they are empty. A few of the very small fluid inclusions in the near vicinity of the monophase fluid inclusions show a very small vapour bubble (2 in Fig. 10d), which persists above the critical temperature of CO_2 (+31 °C) indicating H_2O. The shape and size of the monophase inclusions are similar to type 2 H_2O-CO_2 fluid inclusions, i.e. they may represent decrepitated H_2O-CO_2 fluid inclusions.

In conclusion, the four fluid inclusion types in the host rocks represent three fluids: a low salinity aqueous, a high-salinity brine, and a H_2O-CO_2 fluid. The salinity of the brine fluid cannot be established with great certainty due to extensive modification of the brine fluid inclusions. The formation of the decompression textures did occur at a temperature at ca. 650 °C (Schenk et al., 1991). The fact that the brine fluid inclusions, present in quartz in the decompression rim, was NaCl-saturated at this temperature imposes a minimum salinity of 74 wt% NaCl (NaCl saturation concentration at 650 °C, Steele-MacInnis et al., 2012). However, Hall and Sterner (1993) and Diamond et al. (2010) observed an increase of the salinity due to water loss, which can be up to 20 wt% (Hall and Sterner, 1993). Water loss would have occurred during implosion. Keeping this in mind, it is probably more realistic to assume a minimum salinity of ca. 50 wt% NaCl equivalent for the brine fluid.

4.3. Fluid inclusions in quartz in graphite veins

Indirect evidence on the nature and abundance of fluids of graphite vein formation could be inferred from the vein boundary characteristics and from studying fluid inclusion in quartz that co-precipitated with graphite. Low-salinity aqueous fluid inclusions (type 1) are abundantly present, followed by CO_2 fluid inclusions (type 2). High-salinity brine (type 3), and H_2O-CO_2 fluid inclusions (type 4), on the other hand, are extremely rare.

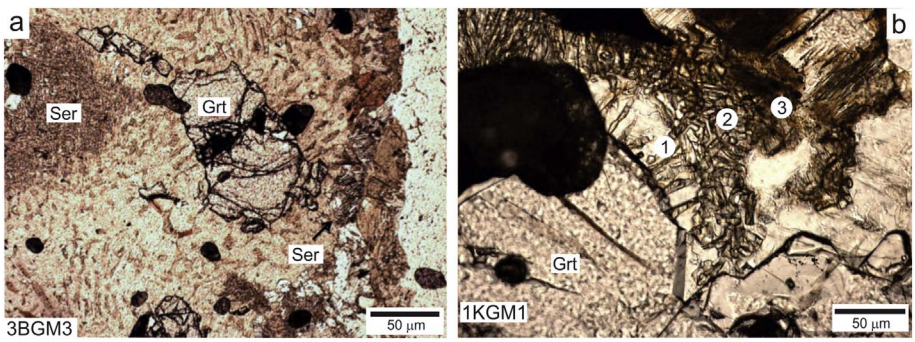

Fig. 9. Photomicrograph (plane polarized light) illustrating alkali metasomatism (see text for discussion). (a) Alteration of plagioclase in a decompression rime (sample 3BGM3 from Bogala). Plagioclase was first altered to antiperthite, which was subsequently altered to sericite. (b) Accumulation of orthopyroxene as a result of leaching out of plagioclase. 1: plagioclase and parallel orthopyroxene needles growing perpendicular to the grain boundary of garnet; 2: accumulation of orthopyroxene crystals; 3: biotite and chlorite.

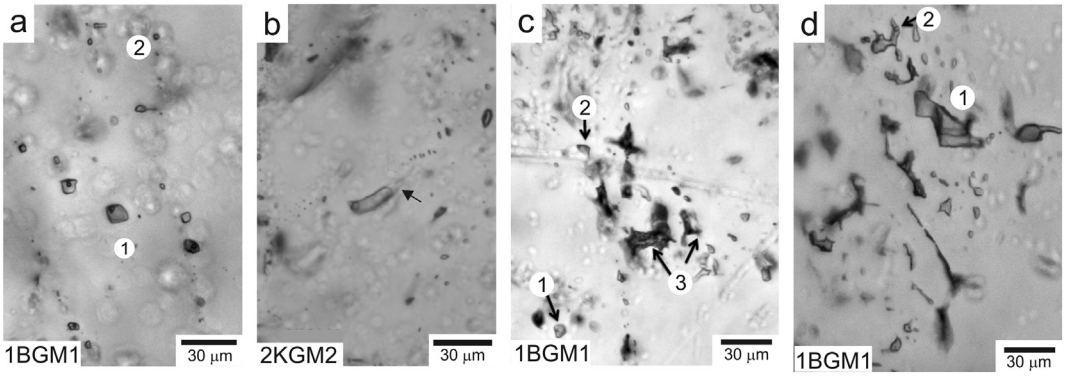

Fig. 10. Illustration of fluid inclusions in host rock samples. (a) Isolated (1) and intragranular trails (2) of low-salinity aqueous fluid inclusions (sample 1BGM1 from Bogala). (b) Large isolated H_2O-CO_2 fluid inclusion (sample 2KGM2 from Kahatagaha). The arrow points to the very faint outline of the aqueous phase. (c) Decrepitated brine fluid inclusions (sample 1BGM1 from Bogala). 1: Very small satellite liquid-vapour fluid inclusion with a halite cube; 2: decrepitated brine inclusions where the halite cube occupies almost the entire cavity; 3: central large cavity (void) with salt cubes attached to the walls. (d) Monophase inclusions possibly representing decrepitated H_2O-CO_2 fluid inclusions (sample 1BGM1 from Bogala). 1: irregular, large central cavity which is either empty or comprises a low-density CO_2; 2: Satellite aqueous liquid-vapour inclusions (very small vapour bubble).

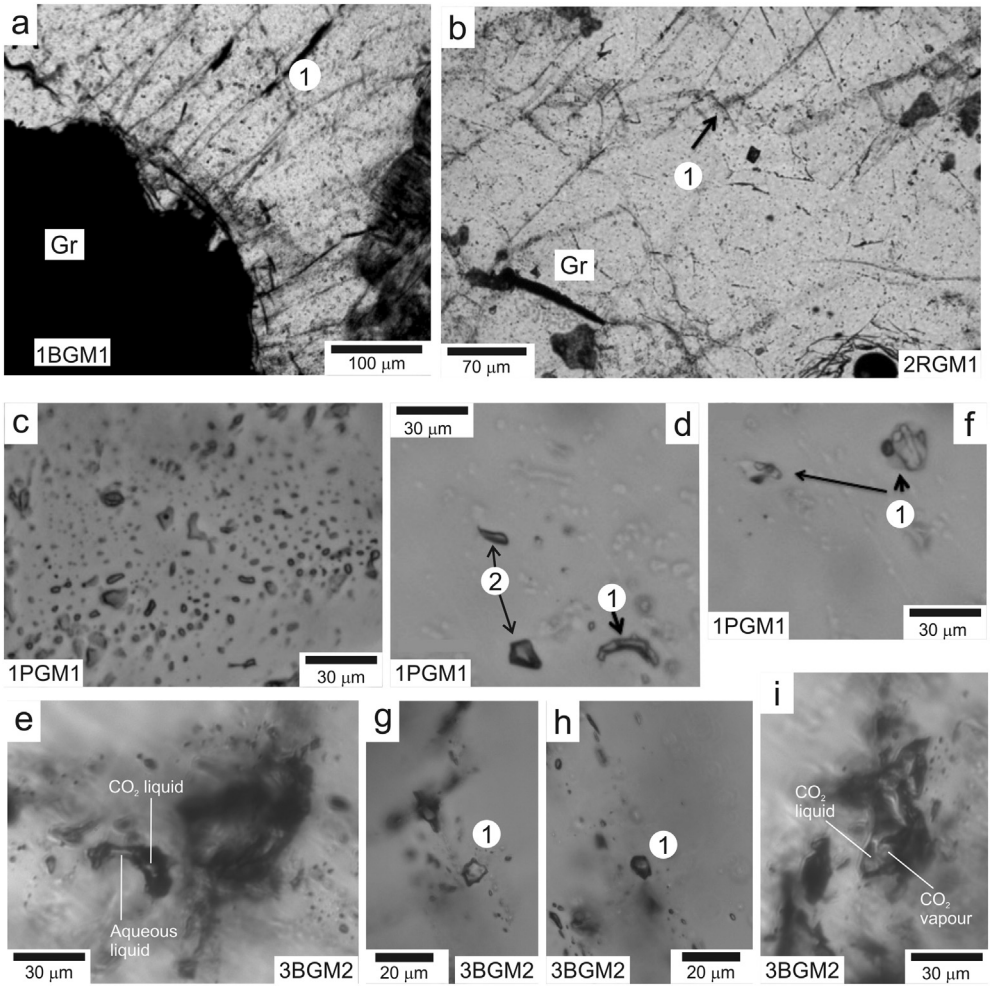

Fig. 11. (a) Sample 1BGM1 from Bogala showing graphite bulge at contact graphite vein-host rock contact (cf. Fig. 4c). Quartz shows radial microfractures with some of them containing elongated graphite veinlets. (b) Sample 2RGM1 from Rangala showing quartz in a graphite vein. The quartz shows in greyish zones defined by (1) a large amount of very small fluid inclusions and graphite crystals (Gr). (c) Clusters and intragranular trails of low-salinity aqueous fluid inclusion in sample 1PGM1. (d) Monophase low-density CO_2 vapour inclusions (1) and circular-shaped CO_2-H_2O fluid inclusion (2) in sample 1PGM1. (e) Cluster of highly irregular shaped CO_2 and H_2O-CO_2 fluid inclusions in sample 3BGM2. (f) Rounded collapsed brine fluid inclusion in sample 1PGM1. Note the squeezed bubble in between the cavity wall and solid phases in the fluid inclusions. (g) Transparent CO_2 fluid inclusion (1) in sample 3BGM2 in the near vicinity of the fluid inclusion shown in (g). Irregular shaped CO_2 fluid inclusion (Th = +3.8 °C into the liquid phase) surrounded by tiny CO_2 fluid inclusions (Th into the liquid phase > +10 °C), indicating partial decrepitation. (h) CO_2 fluid inclusions (1) in sample 3BGM2. The regular-shaped fluid inclusion shows liquid homogenization at a temperature of −27.5 °C. (i) Highly irregular shaped H_2O-CO_2 fluid inclusion at +6 °C. See text for further discussion of this fluid inclusion.

Sample 1BGM1 (contact between the graphite vein and the host rock, Fig. 4a, c) shows radiating microfractures developed in quartz around graphite. Some of these fractures comprise elongated graphite flakes (1 in Fig. 11a). The radiating microfractures are parallel with transgranular trails of type 1 aqueous liquid-vapour fluid inclusions (1 in Fig. 11b). These small (< 10 µm) low-salinity aqueous fluid inclusions (final melting of ice between −1 and 0 °C, indicating a maximum salinity of 2 wt% NaCl) appear to be identical to the ones found in the host rock samples.

Inside the graphite veins, quartz occurs as nodular segregations or short veins interstratified in massive graphite (sample 2RGM1, Fig. 11a). Most quartz crystals appear milky caused by greyish linear zones (1 in Fig. 11b) comprising elongated variably sized graphite crystals and many tiny fluid inclusions (a few microns in size). Despite the small size of the fluid inclusions, a small vapour bubble that exists at temperatures above +31 °C (critical temperature of CO_2) is present. These fluid inclusion trails are, therefore, most likely identical to the low-salinity aqueous fluid inclusions associated with the radiating

microfractures outside of the vein (Fig. 11b). Similar aqueous fluid inclusions were also found in other samples (e.g., sample 1PGM1, Fig. 11c). In sample 3BGM2, large irregular shaped (20–40 μm) low-salinity aqueous fluid inclusions were found and are always associated with type 4 CO_2 fluid inclusions (see below).

Rare isolated H_2O-CO_2 fluid inclusions (type 2) were found in sample 1PGM1 (1 in Fig. 11d) and in sample 3BGM2 (Fig. 11e). Measuring phase transitions during heating-freezing experiments is in most cases impossible due to observation difficulties. However, the H_2O-CO_2 fluid inclusion shown in Fig. 11e showed melting of solid CO_2 at the triple point of −56.6 °C indicating pure CO_2. Final melting of ice at between ca. −1 and 0 °C, and clathrate dissociation at +10 °C indicates a low salinity of the aqueous phase (< 2 wt. NaCl). Similar trailbound H_2O-CO_2 fluid inclusions associated with graphite-bearing inclusions were also observed in quartz associated with graphite from Bogola (Luque et al., 2014).

Isolated, regular-shaped (20–30 μm) brine inclusions (type 3) were found in quartz in a graphite vein (e.g., sample 1PGM1 from Paragoda Mine, 1 in Fig. 11f) and are, similar to the H_2O-CO_2 fluid inclusions, rare. The cavities found within quartz are squeezed around a number of solids that occupies most of the available space. An almost invisible liquid film is visible along the cavity walls and a small deformed vapour bubble is squeezed in between the solids and the cavity walls. This is a typical texture of a collapsed (imploded) fluid inclusion (Touret, 2001).

Monophase liquid and liquid-vapour CO_2 fluid inclusions (type 4) were found in sample 3BGM2 (Fig. 11g, h) occurring either in clusters or in intragranular trails. Relatively large CO_2 fluid inclusions (20–40 μm) are irregular shaped whereas small ones (< 10–20 μm) show regular shapes. Melting of solid CO_2 between −56.6 and −56.7 °C indicates nearly pure CO_2 (Thiéry et al., 1994). Raman analysis of a high-density fluid inclusion (*Th* = −27.5 °C into the liquid phase) that showed melting at −56.7 °C confirms the presence of CH_4. However, the mole ratio CO_2 / (CO_2 + CH_4) must be very close to unity as the melting point is very close to the CO_2 triple point (Thiéry et al., 1994). Liquid homogenization temperature varies widely between −28 and +30 °C indicating densities varying between 1.07 g/cm^3 (41.2 cm^3/mol) and 0.54 g/cm^3 (71.1 cm^3/mol). Very small CO_2 fluid inclusions (< 5 μm) are typically associated with larger CO_2 fluid inclusions and have a lower density than the larger fluid inclusion (Fig. 11g).

Clustered, dark monophase inclusions (type 5) were found in samples 1BGM1 and 1PGM1 (2 in Fig. 11d) and appear to be similar to the type 4 fluid inclusions in the host rocks, i.e. they are either empty or comprise very low density CO_2. The occurrence of small aqueous fluid inclusions within the clusters (sample 1PGM1) suggests that the aqueous and these monophase fluid inclusions were possibly formed as a result of partial decrepitation (i.e., H_2O leakage, Bodnar, 2003) of former H_2O-CO_2 inclusions.

4.4. Summary and discussion of results

In conclusion, the most significant result of this study is the contrast between fluids found in the graphite veins and in the host rocks. Fluid inclusions in the host rock near the graphite veins include high-salinity brine (at least 50 wt% NaCl equivalent), H_2O-CO_2, and low-salinity aqueous fluid inclusions. Quartz in the graphite veins, on the other hand, comprises dominantly low-salinity aqueous fluid inclusions and, to a lesser extent, CO_2 fluid inclusions. Imploded brine and H_2O-CO_2 fluid inclusions are also present but rare. The CO_2 does comprise very small quantities of CH_4, indicated by the slight melting point depression (0.1 °C) and Raman analyses.

The relation between the high-salinity brine fluid and CO_2 is demonstrated by one fluid inclusion found in quartz associated with graphite (sample 3BGM2) (Fig. 11i). This H_2O-CO_2 fluid inclusion comprises pure CO_2 (*Tm* = −56.6 °C, *Th* = ca. +15 °C into the liquid phase) in a high salinity brine. Melting of the aqueous phase could not be measured due to observation difficulties but freezing of the aqueous phase was clearly visible at temperatures between −75 and −85 °C, indicating a salinity of ca. 25 wt% NaCl (Wilkinson, 2017). This fluid inclusion demonstrates that a high-salinity fluid coexisted with CO_2 and that both fluids were heterogeneously trapped under conditions of fluid-fluid immiscibility. The association of irregular shaped relatively large low salinity aqueous fluid inclusions (type 1) with type 4 CO_2 fluid inclusions in sample 3BGM2 indicates refilling of early CO_2 fluid inclusions by a later low salinity aqueous fluid.

The radiating microfractures at the graphite vein-host rock contact indicate that the fluid pressure during the final stage of graphite vein formation was sufficiently high to cause a fracturing of the wall rock and to inject low-salinity aqueous fluids into the host rock. The large abundance of low-salinity aqueous fluid inclusions in quartz in the graphite veins shows that during the final stage of graphite formation, graphite was in quilibrium with a low-salinity H_2O-rich fluid.

5. Formation of graphite veins

5.1. P-T conditions, fluid source, and fluid mobility

The presence of a high-density CO_2 fluid inclusion in quartz in vein graphite from Bogala (Fig. 11g), and the wall-rock alteration assemblage including chlorite and biotite can be used to limit the *P-T* conditions of graphite vein formation. The high-density CO_2 fluid inclusion (*Th* of −27.5 °C into the liquid phase, density of 41.3 g/cm^3) implies a pressure of ca. 7 kbar at ca. 700 °C by extending the WC *P-T* path (Fig. 12). The wall-rock alteration mineral assemblage including biotite and chlorite indicates a relatively low temperature below ca. 500 °C at a pressure of ca. 1–2 kbar according to the WC *P-T* path (Fig. 12). Therefore, graphite formation appears to have started at granulite facies *P-T* conditions and advanced during most of the decompression and cooling stages. This interpretation is supported by the repeated crack-seal process as the mechanism of vein graphite formation (Katz, 1987).

Fluid inclusion data presented in this study and the published stable isotope data reviewed in Section 3 show that vein graphite is primarily formed from CO_2 fluids. The carbon isotope signature (Fig. 5) clearly identifies mantle CO_2 as the primary source. Some of the CO_2 may also have been derived from sedimentary organic matter that reacted with H_2O released from metamorphic dehydration reactions producing CO_2 during prograde metamorphism. Considering the fact that the graphite veins were formed after peak metamorphism, it is highly unlikely that CO_2 was directly derived from the mantle. Therefore, we propose that initially mantle CO_2 was introduced into the lower crust and trapped in UHT granulites during WC-HC collision (Fig. 3a), most likely because of slab breakoff and subsequent upwelling of the mantle asthenosphere (Davies and Von Blanckenburg, 1995). This scenario would also explain post-collisional rapid uplift as depicted in the *P-T* path (Fig. 12, Hiroi et al., 2014; Dharmapriya et al., 2017). The upwelling mantle asthenosphere would result in (1) heat supply to the lower crust causing UHT metamorphism, and (2) concentration of CO_2 into the lower crust (Santosh and Omori, 2008a, 2008b). The CO_2 is derived from decarbonation reactions in the mantle and mobilized along structural discontinuities and/or in magma (Santosh and Omori, 2008a, 2008b). The CO_2 responsible for graphite precipitation was derived from the nearby UHT granulites in central Sri Lanka during decompression at ca. 800 °C (Fig. 12). Decompression associated with fast uplift (Hiroi et al., 2014; Dharmapriya et al., 2017) will mobilize CO_2 (either trapped in fluid inclusions or occurring in isolated pockets) due to the increasing difference between the fast decreasing lithostatic pressure and the fluid pressure. CO_2 fluids have a limited mobility due their high wetting angles (Watson and Brennan, 1987). However, as suggested by Newton and Tsunogae (2014), brines would have enhanced microscale dissolution-precipitation processes (Putnis and Austrheim, 2010) and, therefore, significantly increased the CO_2 mobility laterally and vertically. Both the CO_2 fluid flow and graphite precipitation must have

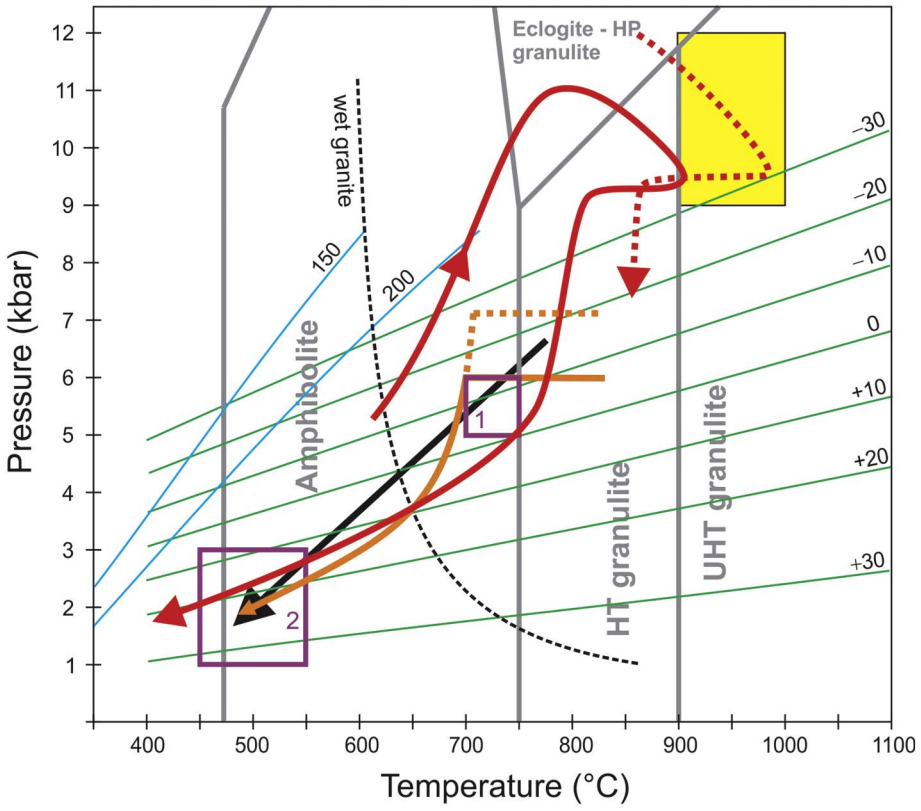

Fig. 12. Pressure-temperature paths constructed for (1) graphite-bearing metapelitic granulite (khondalite) from the HC (red arrow) (Dharmapriya et al., 2017); (2) UHT granulites from the HC (red dashed arrow, Dharmapriya et al., 2015); (3) granulites from the WC (orange arrow, Raase and Schenk, 1994), and (4) arrested charnockite in the WC (Hansen et al., 1987; Sandiford et al., 1988; Schenk et al., 1991; Safonov et al., 1995; Perchuk et al., 2000). Based on the presence of a high-density CO_2 fluid inclusion found in quartz in vein graphite from Bogala (sample 3BGM2, Fig. 11h), we extrapolated the WC *P-T* path to slightly higher pressure conditions (orange dotted line). The yellow box indicates peak *P-T* conditions for the UHT granulites in the HC (Dharmapriya et al., 2015; Osanai et al., 2016a). Purple box 1 indicates the *P-T* conditions of charnockitization (5–6 kbar, 700–750 °C, Perchuk et al., 2000), purple box 2 indicates *P-T* conditions of myrmekite formation in the arrested charnockite (Perchuk et al., 2000). It is noteworthy that the retrograde *P-T* paths of the HC and WC are similar. Metamorphic facies are after Brown (2007). Isochores for CO_2 (green lines) and H_2O (blue lines) for different homogenization temperatures (°C) into the liquid phase are indicated. See text for further discussion. (For interpretation of the references to colour in this figure legend, the reader is referred to the web version of this article.)

been a continuous process while the WC and HC lower crustal rocks were exhumed to middle and shallow crustal levels.

It is expected that the brine and CO_2-rich fluids were focused into narrow fluid pathway zones, a process that was driven by lateral gradients in fluid pressure (Ridley, 1993). Considering the fact that in the middle crust the fluid pressure is equivalent to the lithostatic pressure, lateral variations in the fluid pressure can only be explained by lateral variations in the stress field (Ridley, 1993), such as pre-existing faults or shear zones. The alignment of the graphite deposits roughly parallel to the HC-WC tectonic boundary (Fig. 1) confirms the likelihood of such a scenario.

5.2. Graphite precipitation

Generally, graphite will precipitate from a carbon-oxygen-hydrogen (C-O-H) fluid if the fluid carbon solubility decreases or alternatively if the fluid carbon content increases (Luque et al., 1998; Luque et al., 2014; Huizenga, 2011). Processes that result in a decreased carbon solubility include fluid cooling, or infiltration of the fluid into a more reduced host rock environment. The fluid carbon content increases because of mixing between a CO_2-rich and a CH_4-rich fluid, or alternatively due to removal of H_2O from the fluid phase caused by retrograde hydration reactions (e.g., Luque et al., 1998).

For Sri Lankan graphite we can rule out fluid-fluid mixing as a possible process as no evidence for CH_4-rich fluids was found in any of the studied samples. Fluid cooling, on the other hand, is a distinct possibility (Huizenga, 2011; Luque et al., 2014). The retrograde *P-T* path for the WC (Fig. 12) shows that cooling became significant at temperatures below ca. 650 °C and 3–4 kbar after the initial stage of near-isothermal decompression. During cooling, graphite precipitates according to the net reaction (Huizenga, 2011):

$$CO_2 + 2\,H_2 \rightarrow C + 2\,H_2O \quad (3)$$

Fluid reduction, driven by the redox difference between the relatively oxidized CO_2 fluid and the relatively reduced host rock, is also a possibility (Huizenga and Touret, 2012):

$$CO_2 \rightarrow C + O_2 \quad (4)$$

CO_2 reduction does not require any change in pressure and/or temperature. Therefore, CO_2 reduction was probably the main graphite precipitation process at granulite facies conditions (ca. 700 °C, 7 kbar), i.e. at the start and during the near-isothermal decompression stage of the retrograde *P-T* path. Pyrite is locally associated with Sri Lankan vein graphite (Katz, 1987), which could indicate that pyrrhotite acted as a reducing agent for CO_2. producing graphite and pyrite (e.g., Kirilova et al., 2017).

Both fluid cooling and fluid reduction will lead to a relative increase of the H_2O content in the fluid phase and initiate retrograde hydration reactions (Luque et al., 2014). As mentioned earlier, the graphite veins do show alteration haloes characterized by hydrous mineral phases. The removal of H_2O due to hydration would shift Reaction (3) to the right side causing more graphite to precipitate. Such a feedback system is similar to what was proposed for the Borrowdale graphite deposit in the UK (Ortega et al., 2010). The progress of the hydration reactions will depend on both the temperature and the H_2O activity in the fluid phase.

5.2.1. C-O-H thermodynamic calculations

Thermodynamically calculations allow us to constrain the oxygen fugacity during graphite precipitation (e.g., French, 1966; Ohmoto and Kerrick, 1977; Huizenga, 2001). A carbon-saturated (graphite present) C-O-H fluid has six unknowns at a fixed fluid pressure and temperature including the mole fractions (X) of H_2O, CO_2, CH_4, H_2, CO, and the fluid oxygen fugacity (f_{O_2}) (e.g., French, 1966; Ohmoto and Kerrick, 1977). Four independent equilibria can be written: $CO + 1/2\ O_2 \Leftrightarrow CO_2$, $H_2 + 1/2\ O_2 \Leftrightarrow H_2O$, $CH_4 + 2\ O_2 \Leftrightarrow CO_2 + 2\ H_2O$, and $C + O_2 \Leftrightarrow CO_2$. Further, the sum of the mole fractions (ignoring the extremely low value of X_{O_2}) must be unity: $X_{H_2O} + X_{CO_2} + X_{CH_4} + X_{CO} + X_{H_2} = 1$. Having five equations and six unknowns, we need to fix one compositional variable in order to solve this system. In this case, we can set the $X_{CO_2}/(X_{CO_2} + X_{CH_4})$ ratio to a value very close to unity. In addition, the

Table 3
Thermodynamic data sources and input values used for calculations. See text and Huizenga (2001, 2005) for calculation details.

Thermodynamic data/input	Details/source
Fugacity coefficients for fluid species	Non-ideal mixing equation of state by Zhang and Duan (2009)
Equilibrium constants for reactions in the C-O-H system	Calculated using standard state enthalpy, entropy and isobaric heat capacity from Holland and Powell (2011)
Fayalite-Magnetite-Quartz (FMQ) f_{O_2}	O'Neill (1987), pressure correction by Ballhaus et al. (1991)
P-T values	Retrograde WC *P-T* path (Fig. 12), see Table 4 for specific values
$X_{CO_2}/(X_{CO_2} + X_{CH_4})$	0.99, 0.999, 0.9999

Table 4
Results of thermodynamic calculations. Thermodynamic data and input details are given in Table 3. See text for further explanation.

P-T conditions (kbar, °C)	$X_{CO_2}/(X_{CO_2} + X_{CH_4})$	$\log_{10}f_{O_2}^{fluid} - \log_{10}f_{O_2}^{FMQ}$	X_{H_2O}
7, 700	0.99, 0.999, 0.9999	−0.4, −0.2, −0.1	0.63, 0.24, 0.08
6, 700	0.99, 0.999, 0.9999	−0.5, −0.3, −0.2	0.56, 0.21, 0.07
4, 650	0.99, 0.999, 0.9999	−0.4, −0.3, −0.2	0.48, 0.17, 0.05
3, 600	0.99, 0.999, 0.9999	−0.3, −0.2, −0.1	0.46, 0.16, 0.05
2.5, 550	0.99, 0.999, 0.9999	−0.1, 0.0, +0.1	0.49, 0.16, 0.05
2, 500	0.99, 0.999, 0.9999	+0.1, +0.3, +0.3	0.52, 0.17, 0.05

P-T conditions are constrained by the retrograde *P-T* path of the WC (Fig. 12). Input details and thermodynamic data used for the calculations are summarized in Table 3.

The calculation results are presented in Table 4 and show that both H_2O-CO_2 and CO_2-rich fluids can be expected for oxygen fugacity's that are around the fayalite-magnetite-quartz (FMQ) buffer (FMQ-0.5 < $\log_{10}f_{O_2}$ < FMQ + 0.3). Further, the results also show that relatively small variations in $\log_{10} f_{O_2}$ at fixed *P-T* conditions do have a significant effect on the X_{H_2O} values, which is typical for carbon-saturated binary H_2O-CO_2 mixtures (e.g., Huizenga, 2001). The presence of pure CO_2 and H_2O-CO_2 fluid inclusions with a variable H_2O content can, therefore, be explained by small variations in f_{O_2}.

5.3. Comparison with other graphite deposits in granulite terrains

Granulite-hosted hydrothermal graphite deposits have been reported from southern India (Kerala and Orissa) (Soman et al., 1986; Radhika and Santosh, 1996; Sanyal et al., 2009; Luque et al., 2012, 2014). Similar to Sri Lanka, graphite in those deposits is not related to a specific lithology.

In Kerala, graphite either occurs as disseminated graphite in the host rocks, in shear-related fractures (Radhika and Santosh, 1996), or in pegmatite veins (Soman et al., 1986; Radhika and Santosh, 1996). The association of graphite with pegmatite (Soman et al., 1986; Radhika and Santosh, 1996; Sanyal et al., 2009) indicates high-temperature graphite formation during melt crystallization after peak metamorphism (Luque et al., 2014). The shear zone and pegmatite hosted graphite in southern Kerala shows $\delta^{13}C_{PDB}$ values between −8 and −15‰ whereas the disseminated graphite in the host rocks are much lighter ($\delta^{13}C_{PDB}$ values between −18 and −31‰) (Radhika and Santosh, 1996, and references therein).

In Orissa, graphite occurs in veins and as disseminated flakes in schists. It typically occurs in fractures, fold hinges, and joints (Sanyal et al., 2009). Low $\delta^{13}C_{PDB}$ values are associated with disseminated graphite. Vein graphite, on the other hand, is characterized by heavy carbon ($\delta^{13}C_{PDB}$ values between −2 and −9‰) (Sanyal et al., 2009). Therefore, similar to the graphite deposits in Sri Lanka, the mantle is the most likely carbon source for graphite deposits in southern India. Unfortunately, no fluid inclusion data are available from these deposits.

6. Conclusions

The graphite veins in Sri Lanka are unique because of the large scale of their occurrence and their high crystallinity. Similar graphite veins are found in high-grade metamorphic terranes of southern India (Luque et al., 2014) but at a smaller scale though. This study has shown that a number of factors have contributed to the formation of Sri Lankan vein graphite. Each one is critical in the process, i.e. it is the combination of these factors that allows the formation of these unique deposits. They include: (1) Temporary storage of large amounts of mantle CO_2 in UHT granulites during the continent amalgamation. CO_2 streaming from the mantle asthenosphere (Newton et al., 1980) appears to be typical for UHT granulites (Santosh and Omori, 2008b; Touret and Huizenga, 2012; Touret et al., 2016); (2) Fast exhumation in order to release CO_2 from UHT granulites; (3) Presence of brine fluids to facilitate CO_2 mobility. Brines can also explain the presence of alteration minerals (Rumble, 2014) including Cl-rich biotite, Cl-rich hornblende and Cl-scapolite (Kehelpannala, 1995); (4) Pre-existing structures (e.g., faults, shear zones) that act as fluid focussing zones; (5) Graphite precipitation caused by (a) CO_2 reduction, (b) fluid cooling, and (c) retrograde hydration reactions.

The reason for the high crystallinity of vein graphite in Sri Lanka remains an unresolved issue that is beyond the scope of this paper and requires more research. Luque et al. (2009) demonstrated for the Borrowdale graphite deposit that high crystalline graphite precipitated from a moderate-temperature (ca. 500 °C) fluid, i.e. the crystallinity of hydrothermal graphite appears not to be related to the temperature only (Luque et al., 2014).

Finally, Sri Lankan graphite veins are equivalent to carbonated mega-shear zones found in other granulite terranes (Newton, 1989). Here, the oxidized environment is probably caused by sulphate-bearing brines (Newton and Manning, 2005). In Sri Lanka, the relatively reduced nature of the host rocks allowed the formation of graphite. Large-scale fluid streaming from the mantle (Newton et al., 1980) appears to be typical for UHT granulites, a critical rock type for the amalgamation and disruption of supercontinents (Touret and Huizenga, 2012; Touret et al., 2016).

Acknowledgments

We would like to thank J.P. Gremilliet (Terrae Genesis) for providing thin sections and Alberto Vitale-Brovarone for his help with the microscope photography. JLRT thanks M. Santosh for inviting him to Xian and the ECROFI organizers for their support. KVWK thanks the authorities of Bogala Lanka Graphite Ltd. and the Kahatagaha graphite mine of Sri Lanka for granting him permission to collect samples for this study. Research conducted by JLRT in Paris and KVWK's fieldwork in Sri Lanka, including sample export, were self-sponsored. JMH was funded by James Cook University; FP was funded by Sorbonne University. We would like to thank Elena Crespo Feo, Fons van den Kerkhof, and the guest editor Alexandre Tarantola for their constructive comments and suggestions. This paper is a contribution to the IGCP Project 648 on “Supercontinent Cycles and Global Geodynamics”.

References

Aranovich, L.Ya., Newton, R.C., 1996. H_2O activity in concentrated NaCl solutions at high pressures and temperatures measured by the brucite-periclase equilibrium. Contrib. Mineral. Petrol. 125, 200–212.

Aranovich, L.Y., Newton, R.C., 1999. Experimental determination of CO_2-H_2O activity-composition relations at 600-1000°C and 6-14 kbar by reversed decarbonation and dehydration reactions. Am. Mineral. 84, 1319–1332.

Bakker, R.J., 2003. Package FLUIDS 1. Computer programs for analysis of fluid inclusion data and for modelling bulk fluid properties. Chem. Geol. 94, 3–23.

Ballhaus, C., Berry, R.F., Green, D.H., 1991. High pressure experimental calibration of the olivine-orthopyroxene-spinel oxygen barometer: implications for the oxidation state of the upper mantle. Contrib. Mineral. Petrol. 107, 27–40.

Baur, N., Kröner, A., Liew, T.C., Todt, W., Williams, I.S., Hofmann, A.W., 1991. U-Pb isotopic systematics of zircons from prograde and retrograde transition zones in high-grade orthogneisses, Sri Lanka. J. Geol. 99, 527–545.

Binu-Lal, S.S., Kehekpannala, K.V.W., Satish-Kumar, M., Wada, H., 2003. Multistage graphite precipitation through protracted fluid flow in sheared metagranitoid, Digana, Sri-Lanka: evidence from stable isotopes. Chem. Geol. 197, 253–270.

Bodnar, R.J., 2003. Reequilibration of fluid inclusions. In: Samson, I., Anderson, A., Marshall, D. (Eds.), Fluid Inclusions. Analysis and Interpretation. Min. Ass. Can. Short Course Series Vol. 32. pp. 213–231 (Vancouver).

Bolder-Schrijver, L.J.A., Kriegsmann, L.M., Touret, J.L.R., 2000. Primary carbonate/CO_2 inclusions in sapphirine-bearing granulites from central Sri-Lanka. J. Metamorph. Geol. 18, 259–269.

Brown, M., 2007. Metamorphic conditions in orogenic belts: a record of secular change. Int. Geol. Rev. 49, 193–234.

Burton, K.W., O'Nions, R.K., 1990. The timescale and mechanism of granulite formation at Kurunegala, Sri Lanka. Contrib. Mineral. Petrol. 106, 66–89.

Cesare, B., Ferrero, S., Salvioli-Mariani, E., Pedron, D., Cavallo, A., 2009. Nanogranites and glassy inclusions: the anatectic melt in migmatites and granulites. Geology 37, 627–630.

Clarke, G.L., Norman, A.R., 1993. Pseudotachylite under granulite facies conditions, and its generation during cooling. J. Metamorph. Geol. 11, 319–335.

Cooray, P.G., 1994. The Precambrian of Sri Lanka: an historic review. Precambrian Res. 66, 3–18.

Cordani, U., Cooray, P.G., 1989. Rb-Sr ages of granulites and gneisses from the Precambrian of Sri Lanka. J. Geol. Soc. Sri Lanka 2, 35–43.

Davies, J.H., Von Blanckenburg, F., 1995. Slab breakoff: a model of lithosphere detachment and its test in the magmatism and deformation of collisional orogens. Earth Planet. Sci. Lett. 129, 85–102.

De Maesschalck, A.A., Oen, I.S., Hebeda, E.H., Verschure, R., Arps, E.S., 1990. Rubidium-strontium whole ages of Kataragama and Pottuvil charnockites and Esat Vijayan gneiss: indication of a 2 Ga metamorphism in the highlands of southeast Sri Lanka. J. Geol. 98, 772–779.

Dharmapriya, P.L., 2017. Understanding of ultrahigh temperature lower crustal granulites: implication for P-T-t path and structural evolution of the Highland Complex, Sri Lanka. J. Geol. Soc. Sri Lanka 18, 129–147.

Dharmapriya, P.L., Sanjeewa, P.K., Malaviarachchi, S.P.K., Galli, A., Su, Ben-Xun, Subasinghe, N.D., Dissanayake, C.B., Nimalsiri, T.B., Zhu, B., 2014. *P-T* evolution of a spinel + quartz bearing khondalite from the Highland Complex, Sri-Lanka: implications for non UHT-metamorphism. J. Asia Earth Sci. 95, 99–113.

Dharmapriya, P.L., Malaviarachchi, S.P.K., Galli, A., Su, Ben-Xun, Subbasinghe, N.D., Dissanayake, C.B., 2015. Rare evidence for formation of garnet + corundum during isobaric cooling of ultrahigh temperature metapelites: new insights for retrograde *P-T* trajectory of the Highland Complex, Sri Lanka. Lithos 220–223, 300–317.

Dharmapriya, P.L., Malaviarachchi, S.P.K., Sajeev, K., Zhang, Chengli, 2016. New LA-ICPMS U-Pb geochronology of detrital zircons from the Highland complex: insights into Sri Lanka-India Gondwana linkage. Int. Geol. Rev. 58, 1856–1883.

Dharmapriya, P.L., Malaviarachchi, S.P., Kriegsman, L.M., Galli, A., Sajeev, K., Zhang, C., 2017. New constraints on the *P-T* path of HT/UHT metapelites from the Highland Complex of Sri Lanka. Geosci. Front. 8, 1405–1430.

Diamond, L.W., Tarantola, A., Stünitz, H., 2010. Modification of fluid inclusions in quartz by deviatoric stress. II: experimentally induced changes in inclusion volume and composition. Contrib. Mineral. Petrol. 160, 845–864.

Dissanayake, C.B., 1981. The origin of graphite in Sri Lanka. Org. Geochem. 3, 1–7.

Dobner, A., Graf, W., Hahn-Weinheimer, P., Hirner, A., 1978. Stable carbon isotopes of graphite from Bogala mine, Sri Lanka. Lithos 11, 251–255.

Dunai, T.J., Touret, J.L.R., 1993. A noble gas study of a granulite sample from the Nilgiri Hills, southern India - implications for granulite formation. Earth Planet. Sci. Lett. 119, 271–281.

Elsenheimer, D.W., 1988. Petrologic and Stable Isotopic Characteristics of Graphite and Other Carbon-bearing Minerals in Sri-Lankan Granulites (Unpublished MS thesis). Univ. of Wisconsin-Madison (122 pp).

Fiorentini, E., Hoernes, S., Hoffbauer, R., Vitanage, P.W., 1990. Nature and Scale of Fluid-rock Exchange in Granulite Grade Rocks of Sri Lanka: A Stable Isotope Study. In: Vielzeuf, D., Vidal, P.H. (Eds.), Granulites and Crustal Evolution. Kluwer Academic Publishing, Netherlands, pp. 311–338.

French, B.M., 1966. Some geological implications of equilibrium between graphite and a C-O-H gas at high temperatures and pressures. Rev. Geophys. 4, 223–253.

Gibert, F., Guillaume, D., Laporte, D., 1998. Importance of fluid immiscibility in the H_2O-NaCl-CO_2 system and selective CO_2 entrapment in granulites; experimental phase diagram at 5–7 kbar, 900 °C and wetting textures. Eur. J. Mineral. 10, 1109–1123.

Hall, D.L., Sterner, S.M., 1993. Preferential water loss from synthetic fluid inclusions. Contrib. Mineral. Petrol. 114, 489–500.

Hansen, E.C., Janardhan, A.S., Newton, R.C., Prame, W.K.B.N., Ravindra Kumar, G.R., 1987. Arrested charnockite formation in southern India and Sri Lanka. Contrib. Mineral. Petrol. 96, 225–244.

Harlov, D.E., Hansen, E.C., Bigler, C., 1998. Petrologic evidence for K-feldspar metasomatism in granulite facies rocks. Chem. Geol. 151, 373–386.

He, X.-F., Santosh, M., Tsunogae, T., Malaviarachchi, S.P.K., 2015. Early to late Neoproterozoic magmatism and magma mixing-mingling in Sri-Lanka. Implications for convergent margin processes during Gondwana assembly. Gondwana Res. 32, 151–180.

He, X.-F., Santosh, M., Tsunogae, T., Malaviarachchi, S.P.K., Dharmapriya, P.L., 2016. Neoproterozoic arc accretion along the eastern suture in Sri-Lanka during Gondwana assembly. Precambrian Res. 279, 57–80.

Hiroi, Y., Yanagi, A., Kato, M., Kobayashi, T., Prame, B., Hokada, T., Satish-Kumar, M., Ishikawa, M., Adachi, T., Osanai, Y., Motoyoshi, Y., Shiraishi, K., 2014. Supercooled melt inclusions in lower-crustal granulites as a consequence of rapid exhumation by channel flow. Gondwana Res. 25, 226–234.

Hoefs, J., Touret, J.L.R., 1975. Fluid inclusion and carbon isotope study from Bamble granulites (South Norway). Contrib. Mineral. Petrol. 52, 165–174.

Hoernes, S., Fiorentini, E., Hoffbauer, R., 1994. The role of fluids in granulite-facies metamorphism as deduced from oxygen and carbon isotopic compositions. Precambrian Res. 66, 183–198.

Holland, T.J.B., Powell, R., 2011. An improved and extended internally consistent thermodynamic dataset for phases of petrological interest, involving a new equation of state for solids. J. Metamorph. Geol. 29, 333–383.

Huizenga, J.M., 2001. Thermodynamic modelling of C-O-H fluids. Lithos 55, 101–114.

Huizenga, J.M., 2005. COH, an excel spreadsheet for composition calculations in the C-O-H fluid system. Comput. Geosci. 31, 797–800.

Huizenga, J.M., 2011. Thermodynamic modelling of a cooling C-O-H fluid-graphite system: implications for hydrothermal graphite precipitation. Mineral. Deposita 46, 23–33.

Huizenga, J.M., Touret, J.L.R., 2012. Granulites, CO_2 and graphite. Gondwana Res. 22, 799–809.

Jackson, D.H., Mattey, D.P., Harris, N.B.W., 1988. Carbon isotope compositions of fluid inclusions in charnockites from southern India. Nature 333, 167–170.

Katz, M.B., 1987. Graphite deposits from Sri-Lanka: a consequence of granulite facies metamorphism. Mineral. Deposita 22, 18–25.

Kehelpannala, K.V.W., 1993. Structural Evolution in the Area Surrounding the Kahatagaha-Kolongaha Graphite Mines, North-northwest of Kandy, and the Origin of Vein Graphite of Sri Lanka (Ph.D. thesis (unpublished)). University of Mainz, West Germany (344 pp.).

Kehelpannala, K.V.W., 1995. Origin of vein graphite: another view. In: Dahanayake, K. (Ed.), Handbook on Geology and Mineral Resources of Sri Lanka Second South Asia Geological Congress, Colombo, Sri Lanka. Geol. Surv. & Mines Bureau, Sri Lanka, pp. 95–104.

Kehelpannala, K.W., 1997. Deformation of a high-grade Gondwana fragment, Sri-Lanka. Gondwana Res. 1, 47–68.

Kehelpannala, K.V.W., 1999a. Epigenetic vein graphite mineralization in the granulite terrain of Sri-Lanka. Gondwana Res. 4, 654–657.

Kehelpannala, K.V.W., 1999b. Shear-zone controlled arrested charnockitization, retrogression and metasomatism of high-grade rocks. Gondwana Res. 2, 573–577.

Kehelpannala, K.V.W., 2004. Arc accretion around Sri-Lanka during the assembly of Gondwana. Gondwana Res. 7, 1323–1328.

Kehelpannala, K.V.W., 2017a. Post-metamorphic K-metasomatism of high-grade rocks – a new concept in geology. J. Geol. Soc. Sri Lanka 18, 1–19.

Kehelpannala, K.V.W., 2017b. Graphite occurrences in Sri Lanka. In: Fernando, R., Pitawala, A., Dissanayake, C.B., Dahanayake, K., Jayawardena, D., Wijayananda, N.P. (Eds.), Advancement of Geology in Sri Lanka. Geol. Soc. Sri Lanka (in review).

Kehelpannala, K.V.W., Francis, M.D.P.L., 2001. Vein graphite deposits of the Kegalle District, Sri Lanka: further evidence for post-metamorphic, fluid-assisted graphite. Gondwana Res. 4, 655–656.

Kelsey, D.E., Hand, M.P., 2015. On ultrahigh temperature crustal metamorphism: phase equilibria, trace element thermometry, bulk composition, heat sources, timescales and tectonic settings. Geosci. Front. 6, 311–356.

Kirilova, M., Toy, V.G., Timms, N., Halfpenny, A., Menzies, C., Craw, D., Beyssac, O., Sutherland, R., Townend, J., Boulton, C., Carpenter, B.M., Cooper, A., Grieve, J., Little, T., Morales, L., Morgan, C., Mori, H., Sauer, K.M., Schleicher, A.M., Williams, J., Craw, L., 2017. Textural change of graphitic carbon by tectonic and hydrothermal processes in an active plate boundary fault zone, Alpine Fault, New Zealand. In: Gessner, K., Blenkinsop, T.G., Sorjonen-Ward, P. (Eds.), Characterization of Ore-Forming Systems from Geological. Geochemical and Geophysical Studies 453 Geol. Soc., London, Spec. Publ. http://dx.doi.org/10.1144/SP453.13.

Kleinschrodt, R., 1994. Large-scale thrusting in the lower crustal basement of Sri Lanka. Precambrian Res. 66, 39–57.

Kriegsman, L., Schumacher, J.C., 1999. Petrology of sapphirine-bearing and associated granulites from Central Sri Lanka. J. Petrol. 40, 1211–1239.

Kröner, A., Jaeckel, P., 1994. Zircon ages from rocks of the Wanni complex, Sri Lanka. J. Geol. Soc. Sri Lanka 5, 41–57.

Kröner, A., Williams, I.S., 1993. Age of metamorphism in the high-grade rocks of Sri Lanka. J. Geophys. Res. 101, 513–521.

Kröner, A., Williams, I.S., Compston, W., Baur, N., Vitanage, P.W., Perera, L.R.K., 1987. Zircon ion microprobe dating of high grade rocks in Sri Lanka. J. Geol. 95, 775–791.

Kröner, A., Cooray, P.G., Vitanage, P., 1991. Lithotectonic subdivision of the Precambrian basement of Sri-Lanka. In: Kröner, A. (Ed.), The Crystalline Crust of Sri Lanka. Part I. Vol. 5. Geol. Surv. Dept. Sri Lanka Prof. Paper, pp. 5–21.

Kröner, A., Jaeckel, P., Williams, I.S., 1994. Pb-loss patterns in zircons from a high-grade metamorphic terrain as revealed by different dating methods: U-Pb and Pb-Pb ages for igneous and metamorphic zircons from northern Sri Lanka. Precambrian Res. 66, 151–181.

Kröner, A., Kehepannala, K.W.V., Hegner, E., 2003. Ca. 750–1100 Ma magmatic events and Grenville-age deformation in Sri Lanka: relevance for Rodinia supercontinent formation and dispersal, and Gondwana amalgamation. Precambrian Res. 234, 288–321.

Kröner, A., Rojas-Agramonte, Y., Kehelpannala, K.V.W., Zack, T., Hegner, E., Geng, H.Y., Wong, J., Barth, M., 2013. Age, Nd–Hf isotopes, and geochemistry of theVijayan complex of eastern and southern Sri Lanka: a Grenville-age magmatic arc of unknown derivation. Precambrian Res. 234, 288–321.

Landis, C.A., 1971. Graphitization of dispersed carbonaceous material in metamorphic rocks. Contrib. Mineral. Petrol. 30, 34–45.

Luque, F.J., Pasteris, J.D., Wopenka, B., Rodas, M., Barrenechea, J.F., 1998. Natural fluid deposited graphite: mineralogical characteristics and mechanisms of formation. Am. J. Sci. 298, 471–498.

Luque, F.J., Ortega, L., Barrenechea, J.F., Millward, D., Beyssac, O., Huizenga, J.-M., 2009. Deposition of highly crystalline graphite from moderate-temperature fluids. Geology 37, 275–278.

Luque, F.J., Crespo-Feo, E., Barrenechea, J.F., Ortega, L., 2012. Carbon isotopes of graphite: implications on fluid history. Geosci. Front. 3, 197–207.

Luque, F.J., Huizenga, J.M., Crespo-Feo, E., Wada, H., Ortega, L., Barrenechea, J.T., 2014. Vein graphite deposits: geological settings, origin, and economic significance. Mineral. Deposita 49, 261–277.

Milisenda, C.C., Liew, T.C., Hofmann, A.W., Kröner, A., 1988. Isotopic mapping of age provinces in Precambrian high-grade terrains. J. Geol. 96, 608–615.

Milisenda, C.C., Liew, T.C., Hofmann, A.W., Köhler, H., 1994. Nd isotopic mapping of the Sri Lankan basement: update, and additional constraints from Sr isotopes. Precambrian Res. 66, 95–110.

Newton, R.C., 1989. Metamorphic fluids in the deep crust. Annu. Rev. Earth Planet. Sci. 17, 385–411.

Newton, R.C., Manning, C.E., 2005. Solubility of anhydrite, $CaSO_4$, in NaCl–H_2O solutions at high pressures and temperatures: applications to fluid-rock interaction. J. Petrol. 46, 701–716.

Newton, R.C., Tsunogae, T., 2014. Incipient charnockites: characterization at the type localities. Precambrian Res. 253, 38–49.

Newton, R.C., Smith, J.V., Windley, B.E., 1980. Carbonic metamorphism, granulites and crustal growth. Nature 288, 45–50.

Nokleberg, W.J., 1973. CO_2 as a source of oxygen in the metasomatism of carbonates. Am. J. Sci. 273, 498–514.

Ohmoto, H., Kerrick, D., 1977. Devolatilization equilibria in graphitic systems. Am. J. Sci. 277, 1013–1044.

O'Neill, H.S.C., 1987. Quartz-fayalite-iron and quartz-fayalite-magnetite equilibria and the free energy formation of fayalite (Fe_2SiO_4) and magnetite (Fe_3O_4). Am. Mineral. 72, 67–75.

Ortega, L., Millward, D., Luque, F.J., Barrenechea, J.F., Beyssac, O., Huizenga, J.M., Rodas, M., Clarke, S.M., 2010. The graphite deposit at Borrowdale (UK): a catastrophic mineralizing event associated with Ordovician magmatism. Geochim. Cosmochim. Acta 74, 2429–2449.

Osanai, Y., Sajeev, K., Owada, M., Kehelpannala, K.W.V., Prame, W.K.B., Nakano, N., Jayatileke, S., 2006. Metamorphic evolution of ultrahigh-temperature and high pressure granulites from Highland Complex, Sri Lanka. J. Asia Earth Sci. 111, 145–156.

Osanai, Y., Sajeev, K., Nakano, N., Kitano, I., Kehelpannala, W.K.V., Kato, R., Adachi, T., Malaviarachchi, S.P.K., 2016a. UHT-granulites of the Highland Complex, Sri-Lanka I: geological and petrological background. J. Mineral. Petrol. Sci. 111, 145–156.

Osanai, Y., Sajeev, K., Nakano, N., Kitano, I., Kehelpannala, W.K.V., Kato, R., Adachi, T., Malaviarachchi, S.P.K., 2016b. UHT granulites of the Highland Complex, Sri-Lanka II: geochronological constraints and implications for Gondwana correlation. J. Mineral. Petrol. Sci. 111, 157–169.

Perchuk, L.L., Safonov, O.G., Gerya, T.V., Fu, B., Harlov, D.E., 2000. Mobility of components in metasomatic transformation and melting of gneisses: an example from Sri-Lanka. Contrib. Mineral. Petrol. 140, 212–232.

Pili, E., Sheppard, S.M., Lardeaux, J.M., 1999. Fluid-rock interaction in the granulites of Madagascar and lithospheric-scale transfer of fluids. Gondwana Res. 2, 341–350.

Putnis, A., Austrheim, H., 2010. Fluid-induced processes: metasomatism and metamorphism. Geofluids 10, 254–269.

Raase, P., Schenk, V., 1994. Petrology of granulite-facies metapelites of the Highland Complex, Sri-Lanka: implications for the metamorphic zonation and the *P-T* path. Precambrian Res. 66, 265–294.

Radhika, U.P., Santosh, M., 1996. Shear-zone hosted graphite in southern Kerela, India: implications for CO_2 infiltration. J. Asian Earth Sci. 3/4, 265–273.

Ridley, J.R., 1993. The relations between mean rock stress and fluid flow in the crust: with reference to vein- and lode-style gold deposits. Ore Geol. Rev. 8, 23–37.

Rumble, D., 2014. Hydrothermal graphitic carbon. Elements 10, 427–433.

Rumble III, D., Duke, E.F., Hoering, T.L., 1986. Hydrothermal graphite in New Hampshire: evidence of carbon mobility during regional metamorphism. Geology 14, 452–455.

Safonov, O.G., Aranovitch, L.Y., 2014. Alkali control of high-grade metamorphism and granitization. Geosci. Front. 5, 701–727.

Safonov, O.G., Valley, J.W., Perchuk, L.L., 1995. Isotopic and compositional characteristics of coexisting minerals from metagabbro, the Highland Complex, Sri Lanka. Petrology 5, 478–486.

Sajeev, K., Osanai, Y., 2004. Ultrahigh-temperature metamorphism (1150 °C, 12 kbar) and multi-stage evolution of Mg, Al rich granulites from the central Highland Complex, Sri Lanka. J. Petrol. 45, 1821–1844.

Sajeev, K., Osanai, Y., Suzuki, S., Kagami, H., 2003. Geochronological evidence for multistage-metamorphic events in ultrahigh-temperature granulites from central Highland Complex, Sri Lanka. Polar Geosc. 16, 137–148.

Sajeev, K., Osanai, Y., Connolly, J.A.D., Suzuki, S., Ishioka, J., Kagami, H., Rino, S., 2007. Extreme crustal metamorphism during a Neoproterozoic event in Sri Lanka, a study of dry mafic granulites. J. Geol. 115, 563–582.

Sajeev, K., Williams, I.S., Osanai, Y., 2010. Sensitive high-resolution ion microprobe U-Pb dating of prograde and retrograde ultrahigh-temperature metamorphism as exemplified by Sri Lankan granulites. Geology 38, 971–974.

Sandiford, M., Powell, R., Martin, S.F., Perera, L.R.K., 1988. Thermal and basic evolution of garnet granulites from Sri Lanka. J. Metamorph. Geol. 6, 351–364.

Santosh, M., Omori, S., 2008a. CO_2 flushing: a plate tectonic perspective. Gondwana Res. 13, 86–102.

Santosh, M., Omori, S., 2008b. CO_2 windows from mantle to atmosphere: a tectonic appraisal of ultrahigh-temperature metamorphism and its link with snowball earth. Gondwana Res. 14, 82–96.

Santosh, M., Wada, H., 1993. Microscale isotopic zonation in graphite crystals: evidence for channelled CO_2 influx in granulites. Earth Planet. Sci. Lett. 119, 19–26.

Santosh, M., Tsunogae, T., Yoshikura, S., 2004. Ultra-high density carbonic fluids in ultra-high temperature crustal metamorphism. J. Mineral. Petrol. Sci. 99, 164–179.

Santosh, M., Tsunogae, T., Malaviarachchi, S.P., Zhang, Z., Ding, H., Tang, L., Dharmapriya, P.L., 2014. Neoproterozoic crustal evolution in Sri Lanka: insights from petrologic, geochemical and zircon U–Pb and Lu–Hf isotopic data and implications for Gondwana assembly. Precambrian Res. 255, 1–29.

Sanyal, P., Acharya, B.C., Bhattacharya, S.K., Sarkar, A., Agrawal, S., Bera, M.K., 2009. Origin of graphite, and temperature of metamorphism in Precambiran eastern Ghats Mobile Belt, Orissa, India: a carbon isotope approach. J. Asia Earth Sci. 36, 252–260.

Schenk, V., Raase, P., Schumacher, R., 1991. Metamorphic zonation and *P-T* history of the Highland Complex in Sri Lanka. In: Kröner, A. (Ed.), The Crystalline Crust of Sri Lanka. Part I. Vol. 5. Geol. Surv. Dept. Sri Lanka Prof. Paper, pp. 150–163.

Soman, K., Lobzova, R.V., Sivadas, K.M., 1986. Geology, genetic types, and origin of graphite in south Kerela, India. Econ. Geol. 81, 997–1002.

Steele-MacInnis, M., Lecumberri-Sanchez, P., Bodnar, R.J., 2012. Hokie_Flincs_H_2O-NaCl: a microsoft excel spreadsheet for interpreting microthermometric data from fluid inclusions based on the PVTX properties of H_2O–NaCl. Comput. Geosci. 49, 334–337.

Thiéry, R., Van den Kerkhof, A.M., Dubessy, J., 1994. vX properties of CH_4-CO_2 and CO_2-N_2 fluid inclusions: modelling for $T < 31$ °C and $P < 400$ bars. Eur. J. Mineral. 6, 753–772.

Touret, J.L.R., 2001. Fluids in metamorphic rocks. Lithos 55, 1–25.

Touret, J.L.R., Hansteen, T.H., 1988. Geothermobarometry and fluid inclusions in a rock from the Doddabetta charnockite complex, Southwest India. Rend. Soc. Ital. Mineral. Petrol. 43, 65–82.

Touret, J.L.R., Huizenga, J.M., 2011. Fluids in granulites. In: Van Reenen, D.D., Kramers, J.D., McCourt, S., Perchuk, L.L. (Eds.), Origin and Evolution of Precambrian High-grade Gneiss Terranes, with Special Emphasis on the Limpopo Complex of Southern Africa. Geol. Soc. Am. Mem Vol. 207. pp. 25–37.

Touret, J.L.R., Huizenga, J.M., 2012. Fluid-assisted granulite metamorphism: a continental journey. Gondwana Res. 21, 224–235.

Touret, J.L.R., Santosh, M., Huizenga, J.M., 2016. High-temperature granulites and supercontinents. Geosci. Front. 7, 101–113.

Touzain, P., Balasooriya, N., Bandaranayake, K., Descolas-Gros, C., 2010. Vein graphite from the Bogala and Kahatagaha-Kolongaha mines, Sri-Lanka: a possible origin. Can. Mineral. 48, 1373–1384.

Van den Kerkhof, A.M., Hein, U.F., 2001. Fluid inclusion petrography. Lithos 55, 27–44.

Watson, E.B., Brennan, J.M., 1987. Fluids in the lithosphere, 1. Experimentally-determined wetting characteristics of CO_2-H_2O fluids and their implications for fluid transport, host-rock physical properties, and fluid inclusion formation. Earth Planet. Sci. Lett. 85, 497–515.

Weis, P.L., Friedman, I., Gleason, J.P., 1981. The origin of epigenetic graphite: evidence from isotopes. Geochim. Cosmochim. Acta 45, 2325–2332.

Whitney, D.L., Evans, B.W., 2010. Abbreviations for names of rock-forming minerals. Am. Mineral. 95, 185–187.

Wijayananda, N.P., 1985. Structural control of graphite mineralization at Kahatagaha-Kolongaha, Sri Lanka. In: Dissanayake, C.B., Cooray, P.G. (Eds.), Recent Advances in the Geology of Sri Lanka. 6. Centre International Pour la Formation et le Echanges Geologiques (CIFIG), Paris, pp. 22–56 (Publication Occasionelle).

Wilkinson, J.J., 2017. Metastable freezing: a new method for the estimation of salinity in aqueous fluid inclusions. Econ. Geol. 112, 185–193.

Willbold, M., Hegner, E., Kleinschrodt, R., Stosch, H.-G., Kehelpannala, K.W.V., Dulski, P., 2004. Geochemical evidence for a Neoproterozoic magmatic continental margin in Sri Lanka - relevance for the Rodinia-Gondwana supercontinent cycle. Precambrian Res. 130, 185–198.

Yoshida, M., Santosh, M., 1994. A tectonic perspective of incipient charnockites in East Gondwana. Precambrian Res. 66, 379–392.

Yoshida, M., Funaki, M., Vitanage, P., 1992. Proterozoic to mesozoic east Gondwana: the juxtaposition of India, Sri Lanka, and Antarctica. Tectonics 11 (381–381).

Zhang, C., Duan, Z., 2009. A model for C-O-H fluid in the Earth's mantle. Geochim. Cosmochim. Acta 73, 2089–2102.